SOURCE DATA

TRANSPARENT PROCESS

THE EMBO JOURNAL

Site-specific ubiquitination of the E3 ligase HOIP regulates apoptosis and immune signaling

Lilian M Fennell[1,†], Carlos Gomez Diaz[1,†] (iD), Luiza Deszcz[1], Anoop Kavirayani[2], David Hoffmann[1], Kota Yanagitani[3], Alexander Schleiffer[1,4] (iD), Karl Mechtler[1,4] (iD), Astrid Hagelkruys[1], Josef Penninger[1,5] (iD) & Fumiyo Ikeda[1,3,*] (iD)

Abstract

HOIP, the catalytic component of the linear ubiquitin chain assembly complex (LUBAC), is a critical regulator of inflammation. However, how HOIP itself is regulated to control inflammatory responses is unclear. Here, we discover that site-specific ubiquitination of K784 within human HOIP promotes tumor necrosis factor (TNF)-induced inflammatory signaling. A HOIP K784R mutant is catalytically active but shows reduced induction of an NF-κB reporter relative to wild-type HOIP. HOIP K784 is evolutionarily conserved, equivalent to HOIP K778 in mice. We generated *Hoip*[K778R/K778R] knock-in mice, which show no overt developmental phenotypes; however, in response to TNF, *Hoip*[K778R/K778R] mouse embryonic fibroblasts display mildly suppressed NF-κB activation and increased apoptotic markers. On the other hand, HOIP K778R enhances the TNF-induced formation of TNFR complex II and an interaction between TNFR complex II and LUBAC. Loss of the LUBAC component SHARPIN leads to embryonic lethality in *Hoip*[K778R/K778R] mice, which is rescued by knockout of TNFR1. We propose that site-specific ubiquitination of HOIP regulates a LUBAC-dependent switch between survival and apoptosis in TNF signaling.

Introduction

The linear ubiquitin chain assembly complex (LUBAC) is a critical regulator of inflammation in humans and mice (Walczak, 2011; Ikeda, 2015; Sasaki & Iwai, 2015; Peltzer & Walczak, 2019). LUBAC influences the inflammatory response by regulating the tumor necrosis factor (TNF)-signaling pathway. Upon TNF binding, the TNF receptor (TNFR) forms TNFR complex I (TNFR1), consisting of TNF receptor type 1-associated DEATH domain (TRADD), receptor-interacting serine/threonine-protein kinase 1 (RIPK1), TNF receptor-associated factor 2 (TRAF2), cellular inhibitor of apoptosis protein (cIAP) 1/2 and LUBAC. TNFR complex I promotes cell survival via downstream signaling cascades such as NF-κB through the key kinase complex IκB kinase (IKK) consisting of IKKα/β and NF-κB essential modifier (NEMO). Post-translational modifications, including ubiquitination, regulate multiple events in this signaling cascade. Linear/Met1-, Lys11-, and Lys63-ubiquitin linkage types regulate the recruitment of specific signaling complexes (Peltzer *et al*, 2016; Witt & Vucic, 2017), whereas Lys48-linked ubiquitin chains trigger degradation by the ubiquitin-proteasome system. As part of TNFR complex I, LUBAC generates linear/Met1-ubiquitin chains on NEMO (Haas *et al*, 2009; Tokunaga *et al*, 2009) and RIPK1 (Gerlach *et al*, 2011) to promote NF-κB signaling. NF-κB activation leads to induction of anti-apoptosis genes such as cellular FLICE-like inhibitory protein (cFLIP), thus known as an anti-apoptosis pathway (Lamkanfi *et al*, 2007; Peltzer & Walczak, 2019).

On the other hand, when the NF-κB pathway is disturbed, TNF can promote apoptosis via formation of the TNFR complex II, which consists of RIPK1, TRADD, FAS-associated death domain (FADD) and caspase 8 (Justus & Ting, 2015; Witt & Vucic, 2017). TNFR complex II formation also appears to be regulated by LUBAC (Asaoka & Ikeda, 2015; Sasaki & Iwai, 2015; Peltzer & Walczak, 2019), but the mechanisms are unclear.

LUBAC consists of the E3 ligase HOIP/RNF31 and two subunits HOIL-1L/RBCK1 and SHARPIN/SIPL1 (Gerlach *et al*, 2011; Ikeda *et al*, 2011; Tokunaga *et al*, 2011; Rittinger & Ikeda, 2017). Genetic loss of HOIP or HOIL-1L triggers embryonic lethality in mice due to upregulation of apoptosis, uncovering their essential roles in mouse embryonic development and cell death regulation (Emmerich *et al*, 2013; Peltzer *et al*, 2014; Meier *et al*, 2015; Hrdinka & Gyrd-Hansen,

1 Institute of Molecular Biotechnology of the Austrian Academy of Sciences (IMBA), Vienna Biocenter (VBC), Vienna, Austria
2 Vienna Biocenter Core Facilities (VBCF), Vienna Biocenter (VBC), Vienna, Austria
3 Medical Institute of Bioregulation (MIB), Kyushu University, Fukuoka, Japan
4 Research Institute of Molecular Pathology (IMP), Vienna Biocenter (VBC), Vienna, Austria
5 Department of Medical Genetics, Life Sciences Institute, University of British Columbia, Vancouver, BC, Canada
*Corresponding author. Tel: +81 92 642 4769; E-mail: fumiyo.ikeda@bioreg.kyushu-u.ac.jp
†These authors contributed equally to this works as first and second author

2017). In contrast, SHARPIN-deficient mice ($Sharpin^{cpdm/cpdm}$) suffer from systemic inflammation accompanied with chronic proliferative dermatitis at the age of 6–8 weeks (Seymour *et al*, 2007; Kumari *et al*, 2014). Skin tissues derived from $Sharpin^{cpdm/cpdm}$ mice show immune cell infiltrations and upregulation of keratinocyte apoptosis (Seymour *et al*, 2007). The inflammatory phenotypes of these genetically modified mice are at least partially rescued by TNFR1 knockout, suggesting that LUBAC attenuates apoptosis downstream of the TNF signaling cascade (Kumari *et al*, 2014; Rickard *et al*, 2014). HOIL-1L and HOIP mutations are observed in patients with autoimmune diseases, implicating LUBAC in the regulation of immune responses in humans (Boisson *et al*, 2012; Boisson *et al*, 2015).

At the molecular level, HOIP is a RING-IBR-RING (RBR) type of E3 ligase that specifically generates linear/Met1-linked ubiquitin chains with SHARPIN and HOIL-1L. Linear ubiquitin chains are atypical chains linked via the C-terminal Gly of one ubiquitin moiety to the N-terminal Met1 of another ubiquitin moiety. The catalytic center of HOIP is in the second RING domain (Stieglitz *et al*, 2012), and the linear Ub chain determining domain (LDD) provides its unique ability to generate linear ubiquitin chains (Smit *et al*, 2012). Thus far, HOIP is the only ligase known to generate linear ubiquitin chains (Kirisako *et al*, 2006; Dove & Klevit, 2017).

In vitro, HOIP requires HOIL-1L or SHARPIN to generate linear ubiquitin chains (Kirisako *et al*, 2006; Gerlach *et al*, 2011; Ikeda *et al*, 2011; Tokunaga *et al*, 2011). However, the HOIP RBR-LDD fragment is active in the absence of HOIL-1L and SHARPIN, suggesting a self-inhibitory mechanism (Smit & Sixma, 2014; Walden & Rittinger, 2018). LUBAC generates linear/Met1 ubiquitin chains at lysine residues on substrates, which depends on HOIL-1L (Smit *et al*, 2013). In cells, HOIP exists mostly in complex with SHARPIN or HOIL-1L (Kirisako *et al*, 2006; Tokunaga *et al*, 2011); thus, the LUBAC complex is expected to be active. Yet, the LUBAC-dependent downstream cascades are dependent on stimuli like TNF. The mechanisms that regulate LUBAC activity are unclear. In particular, it is not known how inflammatory stimuli modulate the interactions between LUBAC and its substrates.

Two deubiquitinases (DUBs), called "OTU DUB with LINear linkage specificity" (OTULIN) and CYLD, hydrolyze linear ubiquitin chains and regulate inflammatory signaling cascades. Both OTULIN and CYLD can form a complex with HOIP (Fiil *et al*, 2013; Keusekotten *et al*, 2013; Elliott *et al*, 2014; Schaeffer *et al*, 2014; Takiuchi *et al*, 2014; Elliott *et al*, 2016; Hrdinka *et al*, 2016; Kupka *et al*, 2016; Wagner *et al*, 2016). However, loss-of-function of OTULIN and CYLD in mice does not result in the expected phenotypes compared with LUBAC-deficient mice (Reiley *et al*, 2006; Zhang *et al*, 2006; Damgaard *et al*, 2016); knock-in mice expressing OTULIN C129A (a dominant negative mutant) are embryonic lethal with increased apoptosis signals, partially overlapping with the phenotypes of HOIP and HOIL-1L knockout mice, and the main phenotype known for CYLD deficient mice is in tumor development (Peltzer *et al*, 2014; Heger *et al*, 2018; Peltzer *et al*, 2018). Recently, it was shown that the OTULIN mutant (Cys129Ala) increases ubiquitination signal of all three LUBAC components in cells (Heger *et al*, 2018). Hyper-ubiquitinated LUBAC in the OTULIN mutant Cys129Ala expressing cells is not recruited to TNFR complex I, leading to suppression of this branch of the TNF-induced signaling cascade (Heger *et al*, 2018).

These observations collectively suggest that LUBAC activity and linear ubiquitination of LUBAC components are tightly regulated.

Yet, the post-translational mechanisms controlling LUBAC and its inflammatory outcomes are poorly understood.

Results

Human HOIP is polyubiquitinated in cells

To investigate how HOIP is regulated by ubiquitination, we transiently expressed Myc-HOIP in HEK293T cells. Linear ubiquitin chains were below the detection limit in HEK293T extracts (Appendix Fig S1A), which may reflect their deubiquitination. To stabilize linear ubiquitin chains, we co-expressed catalytically inactive OTULIN (C129A), which acts as dominant-negative (Fiil *et al*, 2013; Keusekotten *et al*, 2013; Heger *et al*, 2018). In addition, to enrich for proteins modified with linear ubiquitin chains, we performed pulldown assays using a known enrichment matrix called GST-linear-TUBE, which consists of GST fused to three tandem repeats of the linear ubiquitin binding-domain UBAN immobilized on a glutathione sepharose resin (Fig 1A; Asaoka *et al*, 2016). We detected modified HOIP in the pulldown by immunoblotting (Appendix Fig S1A, lane 8, and Fig 1B, lane 1) suggesting that HOIP is ubiquitinated at least partially by linear ubiquitin chains, as reported previously with $Otulin^{C129A/C129A}$ knock-in mouse embryonic fibroblasts (MEFs) (Heger *et al*, 2018).

To verify modification of HOIP, we used the ubiquitin chain restriction (UbiCRest) method (Hospenthal *et al*, 2015), a DUB-based analysis to differentiate the linkage types of ubiquitin chains (Fig 1A). The observed HOIP modification disappeared upon treatment with USP21, which hydrolyzes all linkage types of ubiquitin chains, verifying that the modification is ubiquitination (Fig 1B, lane 4). Treatment with either vOTU, which cleaves Lys-linked ubiquitin chains but not linear ubiquitin chains, or with OTULIN, which specifically cleaves linear ubiquitin chains, partially reduced the modification of HOIP (Fig 1B, lane 2 and 3). These data suggest that HOIP is polyubiquitinated with mixed linkage types of Lys and linear. OTULIN treatment diminished the levels of high-molecular-weight HOIP, suggesting that linear ubiquitin chains are added on the Lys-linked ubiquitin chains.

Using mass spectrometry, we uncovered four ubiquitinated residues within human HOIP: lysine (K)454, K458, K735, K784 (Fig 1C and D, Appendix Fig S1B–D). K454 and K458 are not within any of the annotated HOIP domains and are not well-conserved (Fig 1D, Appendix Fig S1E). In contrast, K784 is within the "In Between Ring fingers" (IBR) domain, and K735 is located within the "Really Interesting New Gene" (RING) 1 domain (Fig 1D), and both residues are conserved in a wide range of species (Fig 1E).

HOIP K784 regulates NF-κB activation without affecting LUBAC complex formation in cells

To evaluate the functional role of these ubiquitination sites in HOIP, we generated HOIP K454R, K458R, K735R, and K784R mutants. Given that LUBAC is a regulator of NF-κB signaling, we examined these HOIP mutants using standard NF-κB reporter assays in which luciferase expression is under the control of NF-κB-response elements. Transfected cells expressed similar levels of wild-type (WT) HOIP, the ubiquitination-site mutants (K454R, K458R, K735R,

Figure 1.

Figure 1. Human HOIP is ubiquitinated at K784 and regulates NF-κB.

A A scheme of procedures for the UbiCRest-based assays employed to analyze HOIP modification with ubiquitin chains. Total cell extracts from HEK293T cells transiently expressing Myc-HOIP and Myc-OTULIN C129A, a catalytic inactive mutant, subjected to GST-linear-TUBE pulldown followed by UbiCRest using recombinant deubiquitinases (vOTU, OTULIN and USP21).

B UbiCRest assays to evaluate ubiquitin chain types on HOIP examined by immunoblotting. Immunoblotting of samples using antibodies as indicated. Ponceau S staining used for monitoring GST-liner-TUBE input. Representative data shown from three independent experiments.

C Mass spectrometry spectra corresponding to a peptide containing HOIP-K784 with double Gly (114 + K).

D Domains of human HOIP and identified ubiquitination sites at K454, K458, K735, and K784.

E Multiple sequence alignment of different HOIP orthologues illustrating the position K735 and K784 according to the ClustalX color scheme. Sequences were retrieved from the NCBI protein database with the following accessions: *Homo sapiens* (NP_060469.4), *Canis lupus* (XP_005623312.1), *Mus musculus* (NP_919327.2), *Monodelphis domestica* (XP_007479924.1), *Xenopus laevis* (NP_001090429.1), *Alligator mississippiensis* (XP_006259801.1), *Takifugu rubripes* (XP_003968217.2), and *Drosophila melanogaster* (NP_723214.2).

F Co-immunoprecipitation analysis of the HOIP K784R mutant with SHARPIN and HOIL-1L using total cell extracts of HEK293T cells transiently expressing Myc-HOIP wild type (WT) or Myc-HOIP-K784R with HOIL-1L-HA and Flag-SHARPIN. Anti-Vinculin antibody was used to monitor protein loading. Representative data shown from three independent experiments.

G Luciferase-based NF-κB gene reporter assays using Myc-HOIP wild type (WT), a catalytic inactive mutant C885A, ubiquitination-site mutants of K454R, K458R, K735R, K784R co-transfected with HOIL-1L-HA and Flag-SHARPIN. Luciferase signal was normalized to an internal Renilla control signal.

Data information: In (G), data are presented as mean ± SD. **$P \leq 0.01$, ****$P \leq 0.0001$ (ANOVA). $n = 4$.
Source data are available online for this figure.

K784R), or a negative control (catalytically inactive mutant, C885A) (Fig 1F, Appendix Fig S1F). As expected, we observed an increased luciferase signal in cells that co-express SHARPIN and HOIL-1L with HOIP WT, but not with HOIP C885A (Fig 1G). The luciferase signal was also significantly reduced in cells co-expressing HOIP K784R, whereas it was significantly increased, albeit mildly, in cells co-expressing HOIP K454R, K458R, or K735R (Fig 1G). We observed similar results in assays without HOIL-1L or SHARPIN (Appendix Fig S1G and H).

We chose to pursue the HOIP K784 site, given that it is conserved and promotes NF-κB signaling. To investigate how linear ubiquitination at K784 affects LUBAC formation, we transiently co-expressed HOIP WT or HOIP K784R with HOIL-1L and SHARPIN in HEK293T cells and analyzed their interactions by co-immunoprecipitation. HOIP WT and HOIP K784R each interacted with HOIL-1L and SHARPIN (Fig 1F), suggesting that HOIP K784R supports LUBAC complex formation in cells. These data suggest that HOIP K784R reduces NF-κB reporter activity without compromising LUBAC complex formation.

HOIP K784R generates unanchored linear ubiquitin chains and ubiquitinates NEMO

According to crystal structure analysis, HOIP K784 is on the surface of an alpha helix in the IBR domain, not in contact with the E2 (UbcH5) or the ubiquitin loaded on E2, and distant from the active site C885 (Lechtenberg *et al*, 2016). To determine how mutations in HOIP affect its activity, we purified recombinant HOIP proteins in various forms and performed *in vitro* ubiquitination assays. As expected, the HOIP C885A catalytic mutant did not generate unanchored linear ubiquitin chains nor did it ubiquitinate NEMO (Fig 2A, Appendix Fig S2). Furthermore, HOIP C885A was not polyubiquitinated (Fig 2A, Appendix Fig S2), suggesting that HOIP is modified dependently on its own catalytic activity *in vitro*. Both HOIP WT and HOIP K784R generated unanchored linear ubiquitin chains and ubiquitinated the LUBAC substrate NEMO, when co-incubated with SHARPIN and HOIL-1L (Fig 2A). In the absence of SHARPIN, the ubiquitination signal was reduced in reactions with HOIP K784R compared to HOIP WT (Appendix Fig S2). These data

suggest that the HOIP K784R mutant, in a complex with both HOIL-1L and SHARPIN, can ubiquitinate substrates *in vitro*, though with altered kinetics compared to HOIP WT.

To test HOIP activity in cells, we transiently expressed HOIP WT, HOIP K784R, or HOIP C885A with HOIL-1L and SHARPIN in HEK293T cells. Cells expressing HOIP WT and HOIP K784R displayed similar levels of linear ubiquitin chains and polyubiquitinated NEMO (Fig 2B), whereas cells expressing HOIP C885A lacked both ubiquitination events. These results collectively indicate that HOIP K784R, as a part of LUBAC, can ubiquitinate NEMO *in vitro* and in cells. The observations of HOIP ubiquitination dependent on its catalytic site C885 (Fig 2A and B) and HOIP ubiquitination by mixed linkage types of chains in cells (Fig 1B) suggest that HOIP ubiquitination is at least partially self-ubiquitination in cells.

Hoip^(K778R/K778R) mice do not have overt developmental defects

Given that human HOIP K784R disrupted NF-κB signaling in the reporter assay without substantially affecting HOIP catalytic activity or LUBAC formation in HEK293T cells, we investigated the endogenous function of HOIP K784 *in vivo*. We used CRISPR-Cas9 to generate homozygous knock-in mice with a substitution at HOIP K778, the equivalent residue to K784 in mice (*Hoip*^(K778R/K778R), Appendix Fig S3A and B). *Hoip*^(K778R/K778R) mice were born at the nearly expected ratio from crosses of *Hoip*^(+/K778R) mice and displayed no obvious developmental phenotypes (Fig 3A and B). These observations are in contrast to HOIP loss-of-function mice, which are embryonic lethal (Emmerich *et al*, 2013; Peltzer *et al*, 2014; Hrdinka & Gyrd-Hansen, 2017).

TNF-induced NF-κB activation is suppressed in *Hoip*^(K778R/K778R) MEFs

To analyze if HOIP K778 is involved in the regulation of TNF-dependent NF-κB signaling, we derived MEF lines from *Hoip*^(+/+) and *Hoip*^(K778R/K778R) mice and stimulated them with TNF (Fig 3C and D, Appendix Fig S3C). We found that TNF-induced phosphorylation of IκB-α is prolonged and degradation of IκB-α was very mildly reduced in *Hoip*^(K778R/K778R) MEFs compared with *Hoip*^(+/+) MEFs
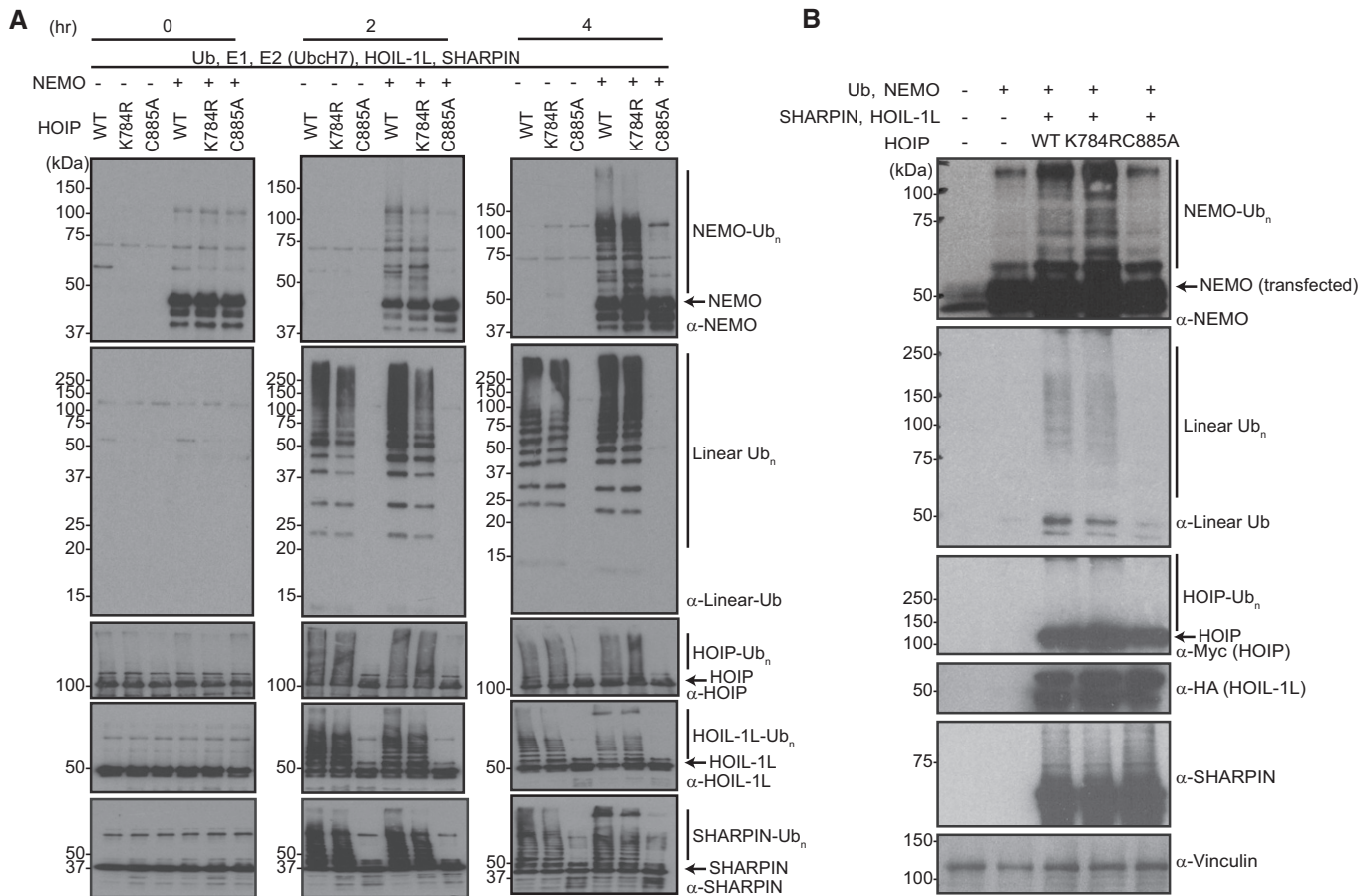
Figure 2. The human HOIP K784R mutant as a part of the LUBAC generates linear ubiquitin chains and ubiquitinates its substrate NEMO *in vitro* and in cells.

A   *In vitro* ubiquitination assays for the indicated times using the recombinant proteins of ubiquitin (Ub), E1, E2 (UbcH7), HOIP (WT, K784R or C885A mutant), HOIL-1L, SHARPIN, and NEMO. Immunoblotting of Linear ubiquitin chains, NEMO, HOIP, HOIL-1L, and SHARPIN detected by using antibodies as indicated. Representative data from three independent experiments.

B   Immunoblotting to detect ubiquitination of NEMO in HEK293T cells transiently expressing Flag-NEMO, GFP-SHARPIN, and HOIL-1L-HA with Myc-HOIP wild-type (WT), Myc-HOIP K784R, or Myc-HOIP C885A. Total cell lysates in denaturing conditions subjected to SDS–PAGE followed up by immunoblotting using antibodies as indicated. Anti-Vinculin antibody was used to monitor loading. Representative data from three independent experiments.

Source data are available online for this figure.

(Fig 3C). In these cells, phosphorylation of IKK was also slightly decreased (Fig 3D). Furthermore, the TNF-induced transcription of some NF-κB target genes, such as ICAM, VCAM, and IκB-α, was significantly reduced in *Hoip*$^{K778R/K778R}$ MEFs compared to *Hoip*$^{+/+}$ MEFs (Fig 3E), whereas TNF-induced gene induction of A20 was unaffected (Appendix Fig S3C).

To elucidate the step of TNF-dependent signaling that is affected in *Hoip*$^{K778R/K778R}$ MEFs, we examined the formation of TNFR complex I. Upon TNF-treatment, RIPK1, HOIP, SHARPIN, and NEMO co-immunoprecipitated with TNF in both *Hoip*$^{+/+}$ and *Hoip*$^{K778R/K778R}$ MEFs (Appendix Fig S3D), indicating recruitment to TNFR complex I. Recruitment of RIPK1, HOIP, and SHARPIN was similar in *Hoip*$^{K778R/K778R}$ MEFs compared to WT MEFs.

Collectively, these data indicate that HOIP K778R mildly but significantly suppresses the TNF-induced NF-κB signaling cascade in MEFs.

Apoptotic markers are increased in *Hoip*$^{K778R/778KR}$ MEFs

LUBAC plays a role in the anti-apoptotic branch of the TNF pathway (Walczak, 2011; Asaoka & Ikeda, 2015; Sasaki & Iwai, 2015). Therefore, we assessed the ability of *Hoip*$^{K778R/K778R}$ MEFs to resist TNF-dependent apoptosis. To this end, we examined TNF-mediated induction of the active form of caspase 3 (cleaved caspase 3), which is a so-called apoptosis executioner caspase, and cleavage of its substrate, PARP (Fig 3F). We also treated cells with cycloheximide (CHX), an inhibitor of translation which sensitizes cells to TNF-induced apoptosis (Rahighi *et al*, 2009; Kumari *et al*, 2014). Compared to *Hoip*$^{+/+}$ MEFs, *Hoip*$^{K778R/K778R}$ MEFs displayed elevated levels of both cleaved caspase 3 and cleaved PARP after treatment with TNF and CHX (Fig 3F). TNF-induced activation of caspase 3 was also measured and quantified by using DEVD-AFC, which emits blue light upon cleavage by activated caspase 3 (Fig 3G). In TNF
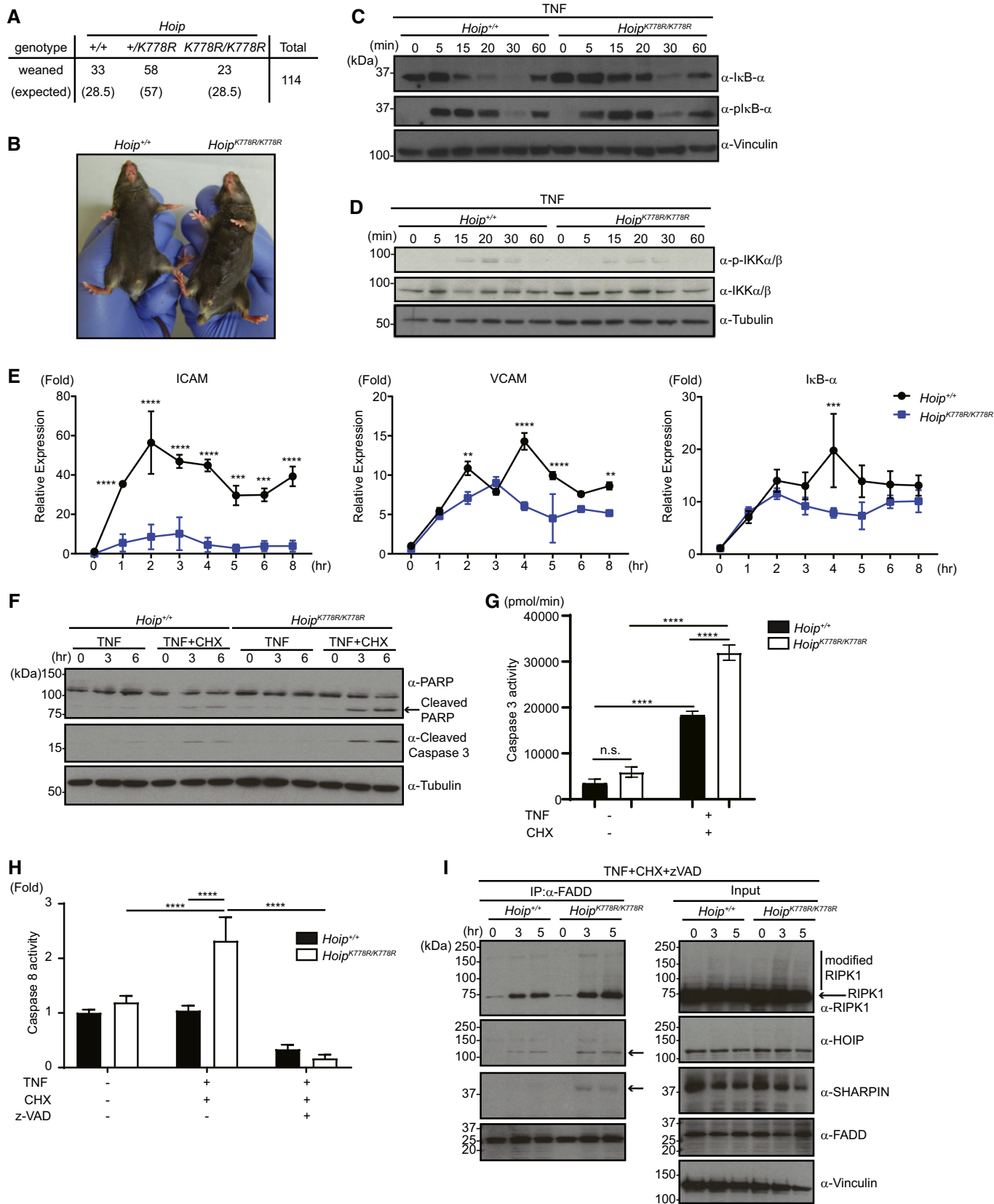
Lilian M Fennell et al

Figure 3.

◀

> **Figure 3. No obvious developmental defect in *Hoip^{K778R/K778R}* knock-in mice is observed while TNF-responses are suppressed in *Hoip^{K778R/K778R}* cells.**
>
> A   Numbers of weaned mice of the indicated genotypes from *Hoip^{+/K778R}* crosses.
>
> B   A gross appearance image of *Hoip^{+/+}* and *Hoip^{K778R/K778R}* male mice at 6 weeks old.
>
> C, D   Immunoblotting to detect TNF-induced degradation and phosphorylation of IκB-α, or phosphorylation of IKK in immortalized *Hoip^{+/+}* and *Hoip^{K778R/K778R}* MEFs treated with human TNF (20 ng/ml) for the indicated times. Immunoblots of anti-Vinculin antibody and anti-α-tubulin antibody shown for monitoring loading amount. Representative data from three independent experiments.
>
> E   Induction of TNF-dependent NF-κB target genes, ICAM, VCAM and IκB-α in *Hoip^{+/+}* or *Hoip^{K778R/K778R}* immortalized MEFs determined by qRT–PCR. RNA extraction and cDNA synthesis from MEFs treated with hTNF (20 ng/ml) for the indicated time subjected to examine transcripts of ICAM, VCAM, and IκB-α. Normalization to β-actin. Representative data from three independent experiments, *n* = 3.
>
> F   TNF-dependent induction of cleavage of PARP and caspase 3 in primary *Hoip^{+/+}* or *Hoip^{K778R/K778R}* MEFs determined by immunoblotting. Total cell extracts of MEFs treated with hTNF (100 ng/ml) and CHX (1 μg/ml) for the indicated times subjected to SDS–PAGE followed by immunoblotting using antibodies as indicated. Anti-α-tubulin antibody was used to monitor loading amount. Representative data of two independent experiments.
>
> G   TNF-dependent induction of caspase 3 activation in immortalized *Hoip^{+/+}* or *Hoip^{K778R/K778R}* MEFs measured by using DEVD-AFC. MEFs treated with hTNF (100 ng/ml) and CHX (1 μg/ml) for 4 h subjected to the caspase 3 activity assays.
>
> H   TNF-induced caspase 8 activity in *Hoip^{+/+}* or *Hoip^{K778R/K778R}* immortalized MEFs treated with hTNF (100 ng/ml) with or without cycloheximide (CHX) (1 μg/ml) or z-VAD (20 μM). Representative data from three independent experiments, *n* = 4.
>
> I   TNF receptor complex II formation in *Hoip^{+/+}* or *Hoip^{K778R/K778R}* immortalized MEFs. Total cell extracts of MEFs treated with hTNF (100 ng/ml), CHX (1 μg/ml) and z-VAD (25 μM) for the indicated time immunoprecipitated using an anti-FADD antibody. Recruitment of RIPK1, HOIP, and SHARPIN monitored by immunoblotting. The anti-Vinculin antibody blot shown for monitoring loading amount. The black arrows indicating HOIP and SHARPIN in the IP samples and unmodified RIPK in the input samples, respectively. Representative data of two independent experiments.
>
> Data information: In (E, G and H), data are presented as mean ± SD. **P ≤ 0.01, ***P ≤ 0.001, ****P ≤ 0.0001 (ANOVA, *n* = 4 in G). CHX (Cycloheximide), hTNF (human Tumor Necrosis Factor), z-VAD (Z-Val-Ala-Asp fluoromethyl ketone).
>
> Source data are available online for this figure.

and CHX-treated *Hoip^{K778R/K778R}* MEFs, DEVD-AFC signal was significantly higher than in *Hoip^{+/+}* MEFs. Similarly, caspase 3 activity measured by live imaging showed that *Hoip^{K778R/K778R}* MEFs treated with TNF or TNF + CHX displayed higher levels of its signal (Appendix Fig S3E, Movies EV1–EV4).

We also measured the activity of an apoptosis initiator caspase, caspase 8, using luminescent assays in *Hoip^{+/+}* and *Hoip^{K778R/K778R}* primary MEFs. We observed significantly higher levels of caspase 8 activity in *Hoip^{K778R/K778R}* MEFs than in *Hoip^{+/+}* MEFs after treatment with TNF and CHX (Fig 3H). Similar responses were observed in MEFs treated with a different cell death ligand, Fas ligand (FasL) (Appendix Fig S3F). As expected, treatment with the pan-caspase inhibitor z-VAD eliminated caspase 8 activity (Fig 3H, Appendix Fig S3F).

TNF- and FasL-induced apoptosis pathways are mediated through the TNFR complex II and the death-inducing signaling complex (DISC), respectively. These signaling pathways have overlapping components including FADD and caspase 8. Thus, we hypothesized that HOIP K778 ubiquitination regulates those cell death-inducing complexes. To address this point, we examined TNFR complex II formation in *Hoip^{+/+}* and *Hoip^{K778R/K778R}* MEFs (Fig 3I). We treated MEFs with TNF, CHX, and z-VAD and immunoprecipitated the TNFR complex II component FADD. We observed an enhanced complex formation between FADD and RIPK1, HOIP, and SHARPIN in *Hoip^{K778R/K778R}* MEFs compared to *Hoip^{+/+}* MEFs. Thus, formation of the TNFR complex II in response to TNF and CHX is elevated in *Hoip^{K778R/K778R}* MEFs compared to *Hoip^{+/+}* MEFs.

Hoip^{K778R/K778R}; *Sharpin^{cpdm/cpdm}* mice display TNFR1-dependent embryonic lethality

Given that *Hoip^{K778R/K778R}* MEFs are sensitized to TNF-induced apoptosis, and that the LUBAC component SHARPIN plays a role in the same apoptosis pathway (Ikeda *et al*, 2011), we investigated a potential cooperation between HOIP and SHARPIN *in vivo*. To this end, we attempted to generate *Hoip^{K778R/K778R}* mice in the

Sharpin^{cpdm/cpdm} background, which do not express functional SHARPIN protein. We did not observe any *Hoip^{K778R/K778R}*; *Sharpin^{cpdm/cpdm}* newborn mice from a cross of *Hoip^{+/K778R}*; *Sharpin^{+/cpdm}* mice (Fig 4A), suggesting embryonic lethality. To examine the embryonic development of *Hoip^{K778R/K778R}*; *Sharpin^{cpdm/cpdm}* mice, we crossed *Hoip^{K778R/K778R}*; *Sharpin^{+/cpdm}* mice and analyzed embryos at E12.5 and E13.5 (Fig 4B and C, Appendix Fig S4A). We observed embryos of all genotypes at both these stages (Fig 4B). However, *Hoip^{K778R/K778R}*; *Sharpin^{cpdm/cpdm}* embryos were found to be unhealthy with grossly evident regions of hemorrhage, suggesting the possibility of lethality at, or immediately subsequent to, these stages (Appendix Fig S4A, Fig 4C).

Sharpin^{cpdm/cpdm} mice display a systemic inflammatory phenotype that requires TNFR1 (Kumari *et al*, 2014; Rickard *et al*, 2014). To elucidate if the embryonic lethality of *Hoip^{K778R/K778R}*; *Sharpin^{cpdm/cpdm}* mice also depends on TNFR1, we tested whether it is rescued by gene knockout of TNFR1. Strikingly, the embryonic lethality is rescued in *Hoip^{K778R/K778R}*; *Sharpin^{cpdm/cpdm}*; *Tnfr1^{−/−}* mice (Fig 4D), and skin inflammation was nearly absent until at least 8 weeks after birth (Fig 4D and E). Furthermore, qualitative reduction of inflammation in tissues such as the lung and liver was also observed in 8-week-old *Hoip^{K778R/K778R}*; *Sharpin^{cpdm/cpdm}*; *Tnfr1^{−/−}* mice, of which inflammatory areas are marked in the panels (Appendix Fig S4B).

Hoip^{+/K778R}; *Sharpin^{cpdm/cpdm}* mice show early onset of severe proliferative dermatitis with keratinocyte apoptosis

Remarkably, heterozygosity of *Hoip^{+/K778R}* was sufficient to bring about an early onset of dermatitis in *Sharpin^{cpdm/cpdm}* mice (Figs 4D and E, and 5A and B). At 4 weeks of age, these mice developed chronic proliferative dermatitis characterized by acanthosis, hyperkeratosis, dermal inflammatory cell infiltrates and keratinocyte apoptosis (detected by cleaved caspase 3 immunostaining). Out of 30 mice of this genotype analyzed, 10 mice survived past 4 weeks: 3 mice to 5 weeks, 3 mice to 6 weeks, and 4 mice to 7 weeks. The

A

Sharpin	Hoip$^{+/+}$			Hoip$^{+/K778R}$			Hoip$^{K778R/K778R}$			Total
	+/+	+/cpdm	cpdm/cpdm	+/+	+/cpdm	cpdm/cpdm	+/+	+/cpdm	cpdm/cpdm	
weaned	10	26	10	12	39	20	3	13	0	133
(expected)	(8.3)	(16.6)	(8.3)	(16.6)	(33.25)	(16.6)	(8.3)	(16.6)	(8.3)	

B

	Hoip$^{K778R/K778R}$			
Sharpin	+/+	+/cpdm	cpdm/cpdm	Total
E12.5	7	11	7	25
(expected)	(6.25)	(12.5)	(6.25)	
E13.5	5	10	5	20
(expected)	(5)	(10)	(5)	

C

D

E
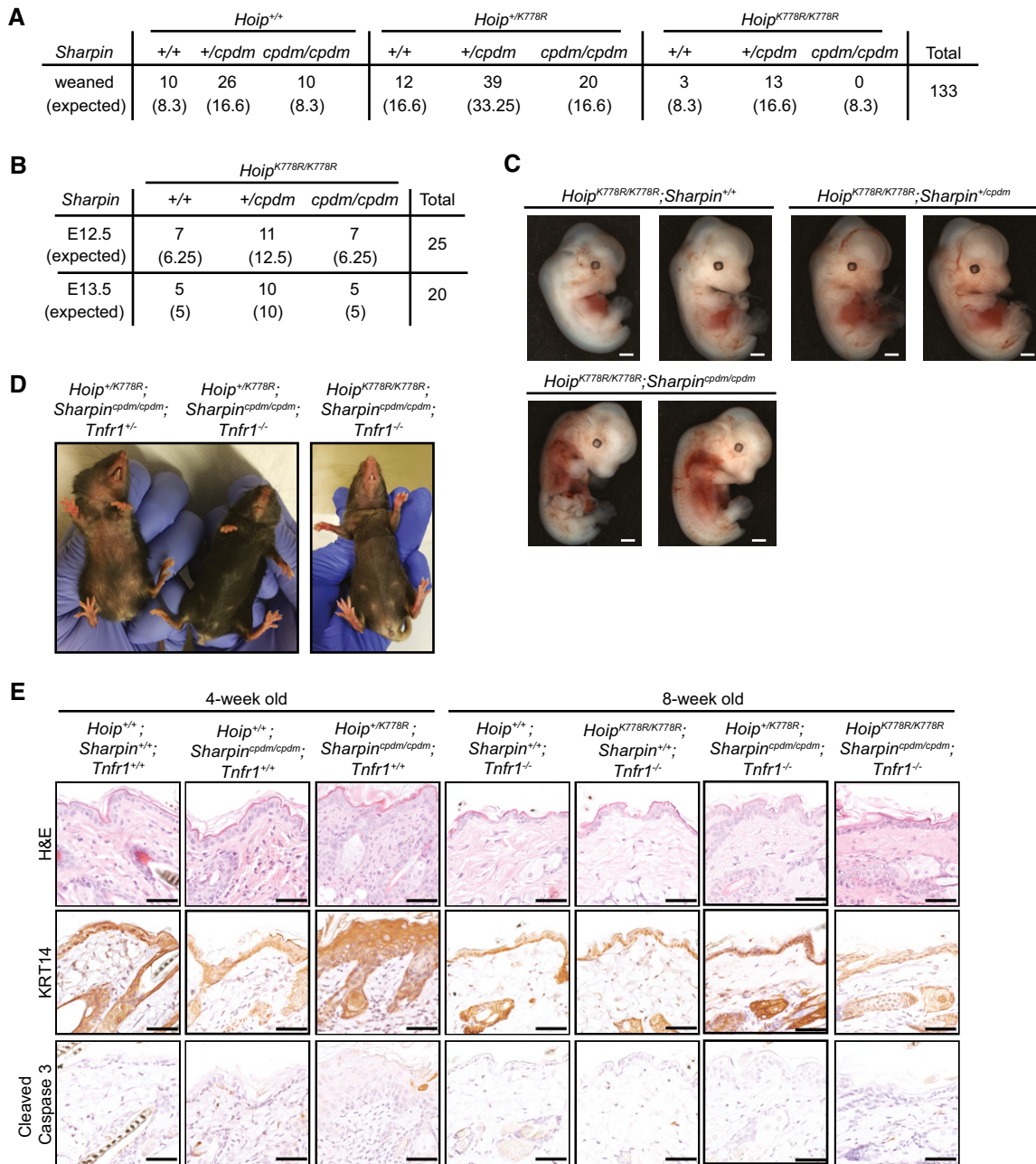
Figure 4. SHARPIN deficiency leads Hoip$^{K778R/K778R}$ mice to embryonic lethality, which is rescued by TNFR1 knockout.

A Numbers of weaned mice of the indicated genotypes from crosses of Hoip$^{+/K778R}$; Sharpin$^{+/cpdm}$ mice.

B Number of the embryos of the indicated genotype at E12.5 and E13.5 from crosses of Hoip$^{K778R/K778R}$; Sharpin$^{+/cpdm}$ mice.

C Gross appearance images of Hoip$^{K778R/K778R}$; Sharpin$^{+/+}$, Hoip$^{K778R/K778R}$; Sharpin$^{+/cpdm}$ and Hoip$^{K778R/K778R}$; Sharpin$^{cpdm/cpdm}$ embryos at E13.5. Representative pictures from 7 embryos each. Scale bars: 1 mm.

D Gross appearance images of Hoip$^{+/K778R}$; Sharpin$^{cpdm/cpdm}$; Tnfr1$^{+/-}$ and Hoip$^{K778R/+}$; Sharpin$^{cpdm/cpdm}$; Tnfr1$^{-/-}$ female mice at 6 weeks of age, and a female Hoip$^{K778R/K778R}$; Sharpin$^{cpdm/cpdm}$; Tnfr1$^{-/-}$ mouse at 8 weeks of age.

E H&E staining, keratin 14 (KRT14) and cleaved caspase 3 immunostaining of dorsal skin sections from mice of the indicated genotypes at 4 or 8 weeks of age. Scale bars: 50 μm.

acanthosis was further confirmed by the thickened keratin 14 (KRT14) positive zone in the epidermis (Fig 4E). In contrast, Hoip$^{+/+}$; Sharpin$^{cpdm/cpdm}$ mice showed no clear sign of skin lesions at this age (Fig 5A and B). The extent of the chronic proliferative

dermatitis in Hoip$^{+/K778R}$; Sharpin$^{cpdm/cpdm}$ mice was further quantified by measurements of total epidermal thickness, keratin layer thickness and squamous epithelial layer thickness (Fig 5C–E). Increased dermal inflammatory cell infiltration in Hoip$^{+/K778R}$;

Sharpin^{cpdm/cpdm} mice was further confirmed by the macrophage marker, F4/80, and the monocyte/granulocyte/neutrophil maker Ly6G (Fig 5B). Importantly, apoptotic epidermal keratinocytes with activated caspase 3 positivity were also prominent in these skin sections (Fig 5B, cleaved caspase 3 panels). These features resemble those of *Sharpin^{cpdm/cpdm}* mice at an older age (8-week old). In addition to the skin, *Hoip^{+/K778R};Sharpin^{cpdm/cpdm}* mice showed a multi-systemic inflammatory phenotype with immune cell infiltrates in visceral organs such as the lung and liver (Appendix Fig S5A). As in *Sharpin^{cpdm/cpdm}* mice, small intestinal Peyer's patches, secondary lymphoid structures, were notably absent in *Hoip^{+/K778R};Sharpin^{cpdm/cpdm}* mice (Appendix Fig S5A). In contrast to the enlarged spleens in *Sharpin^{cpdm/cpdm}* mice, spleens were smaller in *Hoip^{+/K778R};Sharpin^{cpdm/cpdm}* (Appendix Fig S5B). In the spleens of *Sharpin^{cpdm/cpdm}* and *Hoip^{+/K778R};Sharpin^{cpdm/cpdm}* mice, white pulp follicular architecture was obscured in concert with enhanced myeloid hyperplasia in the red pulp (Appendix Figs S5A and B). However, immune phenotyping determined by ELISA using mouse serum (Appendix Fig S5C), or by FACS using spleen and serum (Appendix Figs S6 and S7), did not show very clear differences between *Hoip^{+/+};Sharpin^{cpdm/cpdm}* and *Hoip^{+/K778R};Sharpin^{cpdm/cpdm}* mice. The skin inflammatory phenotype of *Hoip^{+/K778R};Sharpin^{cpdm/cpdm}* mice was mitigated by TNFR1 knockout (Fig 4D and E). These results collectively suggest that ubiquitination of HOIP at K778 in mice collaborates with SHARPIN to regulate TNF-induced inflammation and apoptosis.

To test whether the TNFR1-dependent inflammation and apoptosis phenotypes in *Hoip^{+/K778R};Sharpin^{cpdm/cpdm}* mice are cell autonomous, we established immortalized MEFs and examined TNF-induced signaling cascades, including NF-κB activation and apoptosis (Fig 5F–H). TNF-induced degradation of IκB-α was further delayed in *Hoip^{+/K778R};Sharpin^{cpdm/cpdm}* MEFs, similar to *Hoip^{K778R/K778R}* MEFs and *Sharpin^{cpdm/cpdm}* MEFs (Fig 5F). Cleaved PARP, cleaved caspase 3 by immune blotting, and activated caspase 3 and 8 by activity assays were elevated in *Hoip^{+/K778R};Sharpin^{cpdm/cpdm}* MEFs compared to *Hoip^{+/+}* MEFs, *Hoip^{K778R/K778R}* MEFs and *Sharpin^{cpdm/cpdm}* MEFs treated with TNF, particularly without CHX (Fig 5G–J). We observed similar results with primary ear-derived fibroblasts (Appendix Fig S5D). These results indicate that HOIP ubiquitination at K778 cooperates with SHARPIN to promote TNF-induced cell survival in a cell autonomous manner.

Discussion

Our findings demonstrate that a site-specific ubiquitin modification of HOIP (K784 in human, K778 in mouse) cooperates with SHARPIN to impact TNF-dependent signaling cascades and immune responses in mice (Fig 6). Importantly, HOIP K784R is still ubiquitinated at other sites, both in cells and *in vitro*, emphasizing a specific requirement for ubiquitination at K784 (Fig 2A and B, and Appendix Fig S2). Gene knockout of TNFR1 rescues the mouse phenotypes arising from HOIP K778R and SHARPIN deficiency, indicating the dependency on TNFR1 signaling. The K-to-R substitution in HOIP (K784R in human or K778R in mouse) did not alter HOIP levels, indicating that ubiquitination at this site does not regulate proteasomal degradation.

Hoip^{K778R/K778R} knock-in mice, generated in this study, manifest no overt phenotype for at least 96 weeks after birth. Consistent with our NF-κB gene reporter assays using HOIP K784R, we found that TNF-induced NF-κB activation was mildly suppressed in *Hoip^{K778R/K778R}* cells compared to *Hoip^{+/+}* cells. Apoptosis markers such as active-caspase 3 and 8 induced by TNF and CHX was clearly enhanced in *Hoip^{K778R/K778R}* cells. FADD showed enhanced interactions with RIPK1, HOIP, and SHARPIN in the TNFR complex II in *Hoip^{K778R/K778R}* cells relative to wild-type cells, after treatment with TNF and CHX. These data suggest that ubiquitination of HOIP at K778 (in mice) plays a critical role in the apoptosis pathway by regulating the formation of downstream signaling complexes.

Embryonic lethality was observed in *Hoip^{K778R/K778R}* knock-in mice with concurrent loss of SHARPIN. Additionally, regions of hemorrhage were grossly evident in *Hoip^{K778R/K778R};Sharpin^{cpdm/cpdm}* embryos at the E12.5–E13.5 stages. HOIP and HOIL-1L are critical for embryonic development in mice, and mouse knockouts of these LUBAC components result in hyper-induction of apoptosis in embryos (Peltzer *et al*, 2014; Peltzer *et al*, 2018). This observation was rather a surprise because K-to-R mutation in HOIP did not abolish its activity to generate linear ubiquitin chains, or an overall ubiquitination status of HOIP. Strikingly, a heterozygous allele of *Hoip^{+/K778R}* is sufficient to accelerate skin inflammation and apoptosis in SHARPIN-deficient mice. These data indicate collaborative roles of SHARPIN and HOIP site-specific ubiquitination at K784. The skin inflammatory phenotype in *Hoip^{+/K778R};Sharpin^{cpdm/cpdm}* was partially rescued by deletion of TNFR1 in mice, which is different from the observation made in the crosses with *Sharpin^{cpdm/cpdm}* mice (Rickard *et al*, 2014). These observations collectively suggest that ubiquitination at HOIP K778 is also involved in TNF-independent pathways. Indeed, we observed that FasL also induces significant increases of apoptosis markers in *Hoip^{K778R/K778R}* MEFs (Appendix Fig S3E).

Based on the known co-crystal structure of the HOIP-C-terminal fragment with ubiquitin-loaded E2 (UbcH5), HOIP K784 within the IBR domain does not directly contact the ubiquitin or the E2 (Lechtenberg *et al*, 2016). Furthermore, our *in vitro* ubiquitination assays using recombinant LUBAC components suggest that the suppressed activity of the NF-κB gene reporter is not due to substantial loss of LUBAC activity. However, *in vitro* reactions lacking SHARPIN show that linear ubiquitination is reduced with HOIP K784R relative to HOIP WT, which could in part explain why HOIP K784R knock-in mice with no apparent phenotype become embryonic lethal with SHARPIN deficiency. We observed complete loss of ubiquitination of HOIP C885A relative to HOIP WT, indicating that HOIP ubiquitination relies on its catalytic activity. However, the E3 ligases that directly ubiquitinate HOIP in the TNF signaling cascade in cells or linkage types of ubiquitin chains conjugated on HOIP K784 are not known. HOIP is modified by mixed linkage types of linear and Lys-linked ubiquitin chains in cells, suggesting that additional E3 ligases are involved.

A method to generate a ubiquitination mimic of the substrate to directly address the impact of site-specific ubiquitination, especially by "poly"ubiquitination is not yet established. The only established approach is *in vitro* by chemical reactions such as the click chemistry (Rosner *et al*, 2015). Thus, we mutated HOIP K784 to abolish ubiquitination at this site. Although any mutation can yield nonspecific negative effects, HOIP K784R retained catalytic activity but
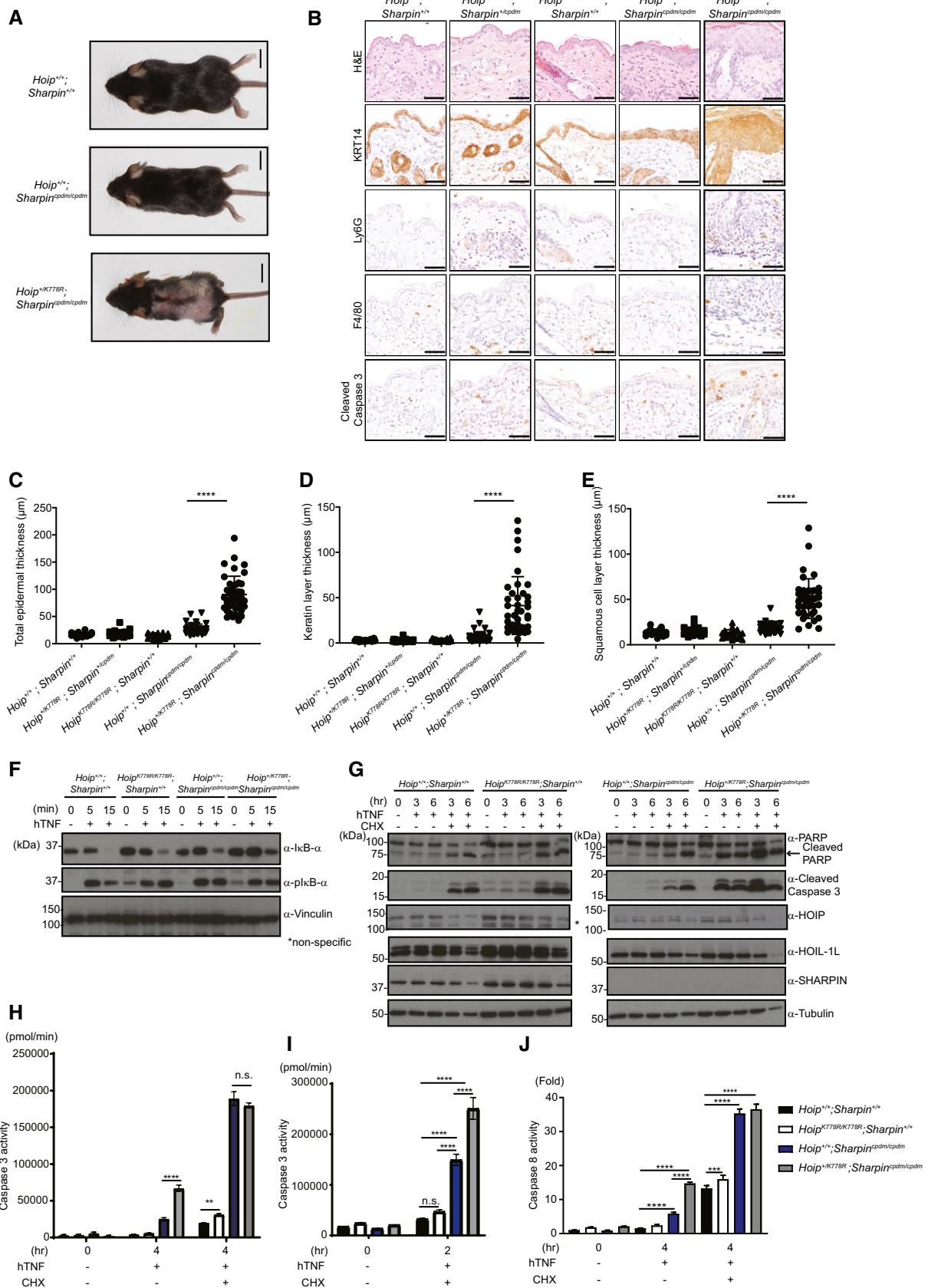
Figure 5.

◀

Figure 5. SHARPIN deficiency in *Hoip*^+/K778R^ heterozygous mice leads to early onset of skin inflammation accompanied with apoptosis induction.

A   Gross appearance of mice of the indicated genotypes (male mice at 4-week old). Scale bars: 10 mm.

B   Immunostaining (H&E, Keratin 14 (KRT14), Ly6G, F4/80 and cleaved caspase 3) of mouse dorsal skin sections of the indicated genotypes. Scale bars: 50 μm.

C–E   Measurements (total epidermis skin thickness, keratin layer thickness and squamous cell layer thickness) of dorsal skin sections obtained from male mice of the indicated genotypes. Each dot on the scatter dot plot represents one focus point of the measurement. (N = 20, 20, 30, 40, 40 for *Hoip*^+/+^; *Sharpin*^+/+^, *Hoip*^K778R/K778R^; *Sharpin*^+/+^, *Hoip*^+/K778R^; *Sharpin*^+/cpdm^, *Hoip*^+/+^; *Sharpin*^cpdm/cpdm^, *Hoip*^+/K778R^; *Sharpin*^cpdm/cpdm^, respectively.)

F   Immunoblotting to examine TNF-induced degradation and phosphorylation of IκB-α in immortalized MEFs of the indicated genotypes using total cell extracts of MEFs treated with hTNF (20 ng/ml) for the indicated times. Representative data from three independent experiments.

G   Immunoblotting of TNF-induced cleavage of PARP and caspase 3 in immortalized MEFs of the indicated genotypes using total cell extracts of MEFs treated with hTNF (100 ng/ml) with or without CHX (1 μg/ml) for indicated times. Representative data from three independent experiments.

H, I   TNF-dependent induction of caspase 3 activation in immortalized MEFs of the indicated genotype measured by DEVD-AFC. MEFs treated with hTNF (100 ng/ml) alone, or with CHX (1 μg/ml) for 4 h (H) or 2 h (I) subjected to the caspase 3 activity assays. A representative data of two independent experiments, n = 4.

J   TNF-induced caspase 8 activity in immortalized MEFs of the indicated genotype. Luminol-dependent activity of caspase 8 in immortalized MEFs treated with hTNF (100 ng/ml) with or without CHX (1 μg/ml). Representative data of three independent experiments, n = 4.

Data information: In (C–E and H–J), data are presented as mean ± SD. **$P \leq 0.01$, ***$P \leq 0.001$, ****$P \leq 0.0001$, ANOVA. hTNF (human Tumor Necrosis Factor), CHX (Cycloheximide).

Source data are available online for this figure.

altered the TNFR complex II formation and function. Thus, the effects we observed with HOIP K784R mutant in cell signaling are not due to non-specific effects on protein folding.

Deubiquitinases are known to regulate HOIP ubiquitination. In a previous study, expression of inactive OTULIN C129A mutant in cells leads to hyper-ubiquitination of LUBAC components, including HOIP, and prevents proper activation of TNF-induced signaling (Fiil *et al*, 2013; Keusekotten *et al*, 2013; Heger *et al*, 2018). In this setting, we observed ubiquitination of HOIP at K784. Although HOIP K784 was shown to be ubiquitinated at the endogenous level (Kim *et al*, 2011; Mertins *et al*, 2013; Akimov *et al*, 2018), in our hands, a peptide containing K784 with ubiquitination signature was only detectable when an inactive OTULIN C129A mutant was expressed in cells. This suggests that overall linear ubiquitination may influence the ubiquitination at HOIP K784. We now show that site-specific ubiquitination of HOIP influenced TNFR complex formation. As a next step, it would be important to understand how the balance of OTULIN and LUBAC is controlled in different cell types to regulate immune responses.

In conclusion, our study has uncovered a new type of regulation of the ubiquitin ligase HOIP by site-specific ubiquitination, which balances inflammatory responses by promoting the formation of TNFR complex I and inhibiting the formation of TNFR complex II. Similar to the regulation of kinases by phosphorylation, site-specific ubiquitin modification of ubiquitin ligases might regulate their activity and function in biology.

Materials and Methods

Plasmids

pBABE-puro-Flag-human SHARPIN, pEGFP-C1-human SHARPIN, pGEX-6P-1-human HOIP, pGEX-4T-1-Linear TUBE, pGEX-6P-1-human OTULIN (WT and C129A), and pcDNA3-human-Ubiquitin were previously described (Ikeda *et al*, 2011; Asaoka *et al*, 2016). pGEX-6P-1-human NEMO, pGEX-6P-1-human HOIL-1L, pGEX-6P-1-human SHARPIN, and pRK5-Myc-human OTULIN (WT and C129A) were cloned using a standard subcloning method. All the point mutants in pcDNA3-Myc-human HOIP (K454R, K458R, K735R, K784R and C885A) and pGEX-6P-1-human HOIP (K784R and

C885A) were generated by site-directed mutagenesis. Sequences of all the plasmids generated for this study were confirmed by Sanger sequencing. pcDNA3-Myc-human HOIP and pcDNA3-human-HOIL-1L-HA were from Kazuhiro Iwai (Tokunaga *et al*, 2009), pGex6P-1-human UbcH7 was from Katrin Rittinger (Stieglitz *et al*, 2012). pOPINK-vOTU (CCHFV OTU, aa1–183) (Addgene plasmid #61589) (Akutsu *et al*, 2011) and pOPINS-USP21 (USP, aa 196–565) (Addgene plasmid #61585) (Ye *et al*, 2011) were gifts from David Komander.

Primer sequences used for the site-directed mutagenesis were the following.

HOIP K454R: forward primer 5′-GCCAGCTCTTTGGAAAGGG GACCCCCCAAG-3′, reverse primer 5′-CTTGGGGGGTCCCCTTTCC AAAGAGCTGGC-3′, HOIP K458R: forward primer 5′-GAAAAGG GACCCCCCAGGCCTGGGCCCCCA-3′, reverse primer 5′-TGGGGGCC CAGGCCTGGGGGGTCCCTTTTC-3′, HOIP K735R: forward primer: CACTTCACCATCGCCTTGAGGGAGAAGCACATC-3′, reverse primer 5′-GATGTGCTTCTCCCTCAAGGCGATGGTGAAGTG-3′, HOIP K784R forward primer 5′-GCGTTGTTCCATAAGAGGCTGACCGAGGG-3′, reverse primer 5′-CCCTCGGTCAGCCTCTTATGGAACAACGC-3′, HOIP C885A: forward primer 5′-GCCCGAGGAGGCGCCATGCACTT TCACTGTACC-3′, reverse primer 5′-GGTACAGTGAAAGTGCATG GCGCCTCCTCGGG-3′.

Antibodies and reagents

The following antibodies were purchased and used according to the manufacturer's instructions: anti-Myc (9E10) antibody (Covance, MMS-150P), anti-HA (HA.11 clone 16B12) antibody (Covance, MMS-101P), anti-Flag (M2) antibody (Sigma, F3165), anti-vinculin antibody (Sigma-Aldrich, V9131), anti-alpha-tubulin antibody (Abcam, ab15246), anti-ubiquitin (P4D1) antibody (Santa Cruz Biotechnology, sc-8017), anti-linear ubiquitin (LUB9) antibody (Life Sensors, #AB130), and anti-linear ubiquitin (LUB4) antibody (a kind gift from Japan Tobacco Inc. Pharmaceutical Frontier laboratories), anti-HOIP antibodies used for the detection of human HOIP (Aviva systems biology, ARP43241_P050, and Sigma, SAB2102031), anti-HOIL-1L antibody (Merck Millipore, MABC576), anti-SHARPIN antibody (Novus, NBP2-04116), anti-Fam105b/OTULIN antibody (Abcam, ab151117), anti-NEMO/IKKγ antibody (FL-419) (Santa Cruz, sc-8330), anti-IκB-α antibody (Cell Signaling, #4812), anti-
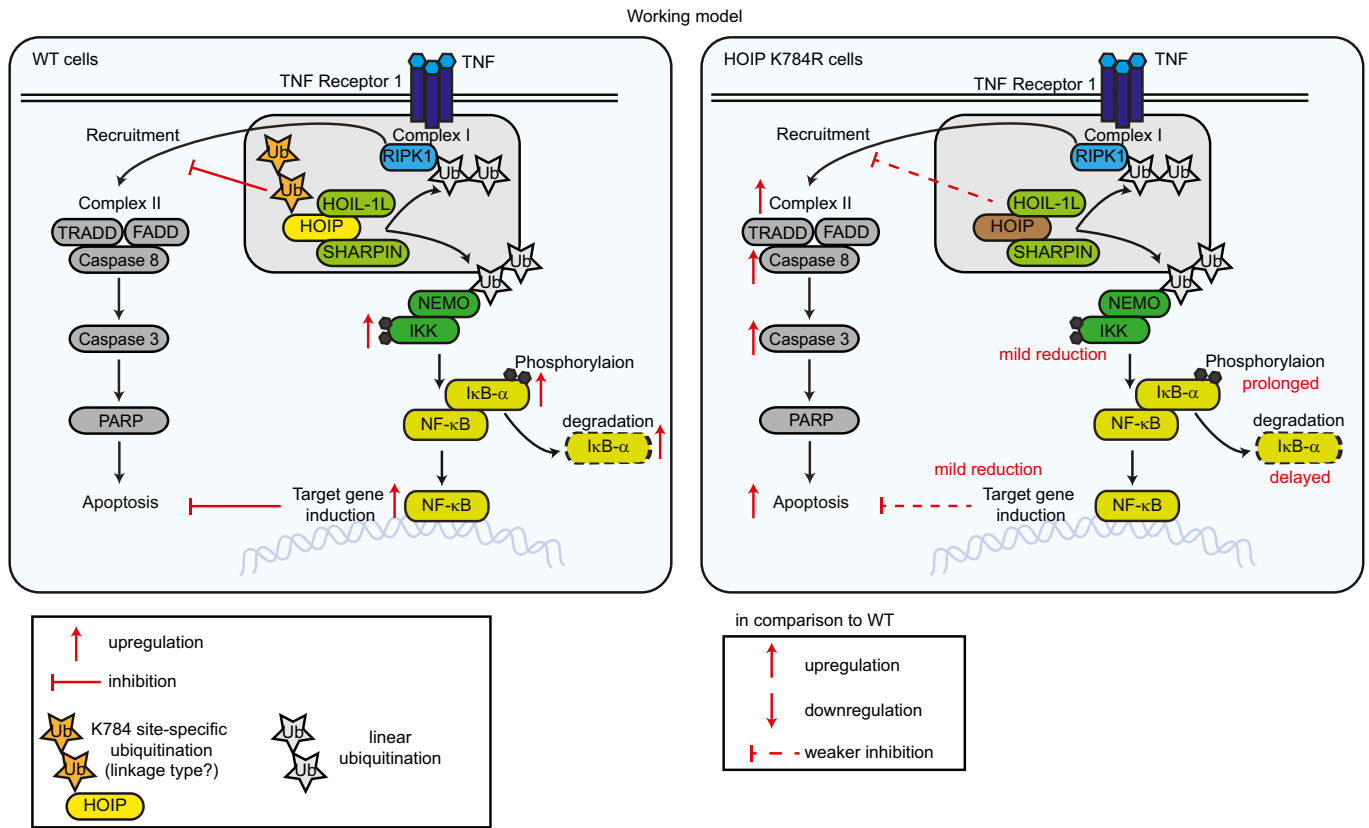
Figure 6. A proposed model of HOIP site-specific ubiquitination in the regulation of the TNF signaling cascades.

A working model describing a role of site-specific ubiquitination of HOIP in the regulation of the TNF-induced NF-κB and apoptosis pathways based on this study. Schematics of simplified TNF signaling in wild-type cells (WT, left panel) and HOIP-K784R cells (right panel) are shown. Upon TNF-binding to TNF receptor 1, complex I, which includes RIPK1 and LUBAC components (HOIP, HOIL-1L and SHARPIN) is formed. In this signaling cascade, LUBAC linearly ubiquitinates NEMO and RIPK1. Site-specific ubiquitination of HOIP at K784 plays a role in inducing TNF-dependent NF-κB target genes and in inhibition of apoptosis by inhibiting RIPK1 recruitment into TNF receptor complex II. Linkage types of ubiquitin chains conjugated on HOIP-K784 remain open.

pIκB-α antibody (Cell Signaling, #9246), anti-IKKα/β antibody (Abcam, EPR16628), anti-pIKK antibody (Cell signaling #2697), anti-PARP antibody (Cell Signaling, #9542), anti-cleaved caspase 3 antibody (Cell Signaling, #9664), anti-FADD antibody used for immunoprecipitation (Santa Cruz, sc-271748), anti-FADD antibody used for detection of FADD by immunoblotting (Abcam, ab124812), and anti-RIPK1 antibody (Cell signaling, #3493). A polyclonal antibody against mouse HOIP was raised against a recombinant protein containing a mouse HOIP fragment (aa 475–625) by immunizing rabbit (immunoGlobe, Germany). Secondary antibodies used for the immunoblotting are Goat anti-Mouse IgG-HRP (Bio-Rad, 170-6516) and goat anti-Rabbit IgG-HRP (Dako, P0448). Secondary antibodies used for immunoprecipitation were Protein G Agarose beads (Roche, 1124323301) and anti-FLAG (M2) beads (Sigma-Aldrich, A2220).

Recombinant human Flag-TNF (Enzo, ALX-522-008-C050), recombinant human TNF (Peprotech, 300-01A), cycloheximide (CHX) (Sigma-Aldrich, C4859) and Z-Val-Ala-DL-Asp(Ome)-fluoromethylketone (z-VAD-fmk) (Bachem, N-1560) were also used. Recombinant Fc-Fas ligand was a kind gift from Pascal Schneider (Schneider *et al*, 1997).

Tissue culture and transfection

Human embryonic kidney 293T (HEK293T) (ATCC) and immortalized MEFs were maintained at 37°C in 5% CO_2 in Dulbecco's modified Eagle's medium (DMEM) (Sigma, D5648) supplemented with 10% fetal calf serum (Thermo Fisher Scientific, 10270106), 1% L-glutamine (Thermo Fisher Scientific, 25030-024), and 1% penicillin–streptomycin (Sigma, P0781). PCR-based mycoplasma tests confirmed all cells to be negative for mycoplasma contamination. Transfections in HEK293T or MEFs were performed using GeneJuice (Merck Millipore, 70967) according to the manufacturer's protocol.

Isolation and immortalization of mouse embryonic fibroblasts (MEFs)

Primary MEFs were isolated from E13.5 embryos (C57BL/6J *Hoip*^{+/+} and *Hoip*[K778R/K778R], C57BL/6J/KaLawRij *Hoip*^{+/+}; *Sharpin*^{+/+}, *Hoip*[K778R/K778R]; *Sharpin*^{+/+}, *Hoip*^{+/+}; *Sharpin*[cpdm/cpdm], and *Hoip*[K778R/+]; *Sharpin*[cpdm/cpdm]) according to a standard protocol (Ikeda *et al*, 2011).

Isolation of primary mouse dermal adult fibroblasts (MDFs)

Primary mouse dermal adult fibroblasts (MDFs) were isolated from ear tissue derived from mice at four weeks of age. Ear tissue was washed in 70% ethanol, air dried, and minced into small pieces using a scalpel. Tissue pieces were collected in Dulbecco's modified Eagle's medium (DMEM) (Sigma, D5648) supplemented with 10% fetal calf serum (Thermo Fisher Scientific, 10270106) 1% penicillin–streptomycin (Sigma, P0781), gentamicin (50 μg/ml) (Thermo Fisher Scientific, 15750060), and 1% MEM non-essential amino acid solution (Thermo Fisher Scientific, 11140050) and centrifuged at 211 RCF for 5 min. Trypsin (Thermo Fisher scientific, 25300054) treated tissue pieces were incubated for 1 h at 37°C, with a vortex step performed every 15 min. Fresh media was added, and the tissue pieces were centrifuged, resuspended in fresh media and plated in a tissue culture dish. MDFs were seeded for cellular assays upon reaching confluency.

Cell lysis

A method is described elsewhere (Ikeda *et al*, 2011). Briefly, cells were lysed in chilled lysis buffer (50 mM HEPES (pH 7.4) (Sigma-Aldrich, H4034), 150 mM NaCl, 1 mM EDTA, 1 mM EGTA, 1% Triton X-100, 10% Glycerol, 25 mM NAF and 10 μM ZnCl2, 1× cOmplete protease inhibitor cocktail (Roche, 11836170001), 1 mM PMSF (Roche, 10837091001) and 10 mM NEM (Sigma-Aldrich, E3876) on ice. Lysates were cleared by centrifugation at 21,130 RCF for 15 min. For denaturing conditions, cells were lysed in 1% SDS-PBS and boiled at 96°C for 10 min as described before (Sasaki *et al*, 2015). Subsequently, lysates were sheared through a 27 3/4G needle (Becton Dickinson, BD 302200) several times, centrifuged at 15,000 rpm for 5 min (at room temperature), and the supernatant was subjected for different assays.

Immunoprecipitation

For immunoprecipitation of Myc-HOIP, anti-Myc antibody (1 μg) was incubated for 2 h at 4°C, followed by incubation with Protein G Agarose beads (Roche, 1124323301) (15 μl) for 2 h at 4°C. Beads were washed four times in lysis buffer. Proteins were eluted from beads using 30 μl of 2× SDS sample buffer and heated at 96°C for 5 min.

A method for immunoprecipitation of the TNFR complex I is described in previous studies (Haas *et al*, 2009; Draber *et al*, 2015). Briefly, after serum starvation in 0.2% FCS-DMEM for 15 h, MEFs ($5–20 × 10^6$ cells) were treated with 1 μg/ml of Flag-human TNF, washed by PBS twice, and lysed in 1 ml of chilled IP-Lysis buffer (30 mM Tris–HCl (pH 7.4), 120 mM NaCl, 2 mM EDTA, 2 mM KCl, 10% glycerol, 1% Trition X-100, 50 mM NaF, 1× cOmplete protease inhibitor cocktail (Roche, 11836170001), 1 mM PMSF (Roche, 10837091001), 10 mM NEM (Sigma-Aldrich, E3876), and 5 mM NAVO$_4$ (Sigma-Aldrich, S6508)) for 30 min on ice. Lysates were centrifuged at 15,000 rpm for 30 min at 4°C. Flag-human TNF (1 μg) was added to the 0 h control samples. After preclearing with Protein G Agarose beads for 1 h at 4°C, anti-FLAG (M2) beads (Sigma-Aldrich, A2220) (10 μl of beads slurry) were incubated for 16 h at 4°C, washed five times with the IP-lysis buffer, and denatured for 5 min at 96°C in 2× SDS sample buffer.

A method for immunoprecipitation of TNFR complex II is described elsewhere (Ang & Ting, 2018). Briefly, MEFs ($5–20 × 10^6$) were treated with human TNF (100 ng/ml), z-VAD-fmk (25 μM), and cyclohex-imide (1 μg/ml) for the indicated times and lysed in chilled DISC-IP buffer (150 mM NaCl, 20 mM Tris–HCl pH 7.5, 1 mM EDTA, 0.2% NP40, 10% glycerol supplemented with cOmplete protease inhibitor cocktail (Roche, 11836170001), 0.1 mM Na$_3$VO$_4$ (Sigma-Aldrich, S6508), 100 mM NEM (Sigma-Aldrich, E3876), 1 mg/ml of BSA (VWR International, 422351S) for 10 min on ice. Lysates were centrifuged at 21,130 RCF for 15 min, and supernatant was precleared with Protein G Agarose beads (25 μl) for 1.5 h at 4°C, followed by immunoprecipitation with α-FADD antibody (2 μg) (Santa Cruz; sc-271748) incubation for 16 h at 4°C. Subsequently, Protein G Agarose beads (25 μl) incubation for 1.5 h at 4°C. Immunoprecipitated samples were washed four times with DISC-IP buffer. Samples were heated at 70°C for 20 min in 2× SDS sample buffer.

GST-Linear TUBE pulldown

GST-Linear TUBE pulldown was performed as previously described (Asaoka *et al*, 2016). Briefly, cells were lysed in mammalian lysis buffer on ice and cleared by centrifugation. GST-empty and GST-Linear TUBE immobilized on glutathione Sepharose 4B beads were incubated with supernatants for 12 h at 4°C. Pulldown samples were washed five times in lysis buffer and heated at 96°C for 5 min in 2× SDS sample buffer.

Immunoblotting

The protocol used for immunoblotting was described previously (Ikeda *et al*, 2011) (Kumari *et al*, 2014). Briefly, samples were resolved by SDS–PAGE and transferred to a nitrocellulose membrane (GE Healthcare, 10600019 or 10600001). The membrane was first stained with Ponceau S (Roth, 5938.1) to monitor the transferred proteins. Membranes were washed, blocked with 5% BSA-TBS, and blotted with the indicated primary antibodies diluted in 5% BSA-TBS at 4°C overnight. Subsequently, membranes were incubated with a secondary antibody according to the manufacturer's instructions, and signal was detected with Western Blotting Luminol Reagent (Santa Cruz; sc-2048) on high-performance chemiluminescence films (GE Healthcare, Amersham Hyperfilm ECL, 28906837).

Luciferase-based NF-κB gene reporter assay

HEK293T cells were seeded in 96-well plates ($1 × 10^4$ cells/well) (Thermo Scientific, 136101) and transfected with pNF-κB-Luc (Stratagene) and phRK-TK (Renilla) (Promega) using GeneJuice (Merck Millipore, 70967). After 48 h, samples were subjected to a luciferase assay using the Dual-Glo Luciferase Assay System (Promega; E2940) according to the manufacture's protocol. Luciferase and Renilla signal were measured by the Synergy H1 hybrid multimode microplate reader (BioTek) and monitored by Gen5 software. Each experimental sample was carried out in quadruplicate and normalized to the Renilla signal.

Protein purification

A method is described elsewhere (Ikeda *et al*, 2011; Asaoka *et al*, 2016). Briefly, plasmids were transformed into BL21 (DE3) *Escherichia coli*. Bacterial cells were grown in the LB media at 37°C.

Expression of GST tagged fusion proteins was induced using 100 μM IPTG (Thermo Scientific, R0392) at OD_{600} = 0.8 in 4–6 liters of culture. 100 μM $ZnCl_2$ (Sigma-Aldrich, 229997) was added during induction of HOIP, HOIL-1L, and SHARPIN expression only. Cultures were grown overnight at 18°C. Cells were centrifuged and resuspended in the suspension buffer (100 mM HEPES (Sigma-Aldrich, H4034), 500 mM NaCl, 1 mM TCEP-HCl (Thermo Scientific, 20491) pH 7.4 which was supplemented with recombinant DNase I (1000 U) (Roche, 04536282001), cOmplete protease EDTA-free inhibitor cocktail (Roche, 11836170001) and 1 mM PMSF (100 mM in isopropanol, Roche, 10837091001). Cells were sonicated and 0.5% Triton X-100 was added to the lysate. The lysate was cleared by centrifugation and applied to a 5 ml GSTrap FF column (GE Healthcare, 17513101) to initially purify GST-proteins. The GST-tag was removed by overnight on-column cleavage with the PreScission Protease (homemade). Protein eluates were further resolved using size exclusion chromatography on gel filtration columns using the Superdex 200 (16/600) (GE Healthcare, GE28-9893-35) or Superdex 75 (16/600) (GE Healthcare, GE28-9893-33) in a buffer containing 50 mM HEPES (Sigma-Aldrich, H4034), 150 mM NaCl, 1 mM TCEP-HCl (Thermo Scientific, 20491), pH 7.4. Eluted fractions were analyzed in SDS–PAGE stained with InstantBlue™ Protein Stain (Expedeon, 1SB1L), and the fractions containing the desired protein were pooled together. Proteins were concentrated using a Vivaspin concentrator (Sartorius) with a half lower MWCO than the size of the protein being purified. Protein concentrations were determined by UV absorption at 280 nm using calculated extinction coefficients or compared to known BSA standards visualized by SDS–PAGE and stained with Instant Blue. A baculovirus for insect expression of His_6- mouse Ube1 in Hi5 cells was a kind gift from Kazuhiro Iwai and was expressed and purified as previously described (Iwai *et al*, 1999).

NanoLC-MS analysis

Samples containing HOIP were separated using SDS–PAGE using 4–15% Mini-PROTEAN TGX gels (Bio-Rad; #4561083). Gels were silver stained according to Blum's protocol (Helmut *et al*, 1987). Gel fragments containing the HOIP band and above were extracted from the gel. Following this, the gel bands were reduced, alkylated and digested with Trypsin.

The nano HPLC system used was an UltiMate 3000 RSLC nano system (Thermo Fisher Scientific, Amsterdam, Netherlands) coupled to a Q Exactive Plus mass spectrometer (Thermo Fisher Scientific, Bremen, Germany), equipped with a Proxeon nanospray source (Thermo Fisher Scientific, Odense, Denmark). Peptides were loaded onto a trap column (Thermo Fisher Scientific, Amsterdam, Netherlands, PepMap C18, 5 mm × 300 μm ID, 5 μm particles, 100 Å pore size) at a flow rate of 25 μl/min using 0.1% TFA as mobile phase. After 10 min, the trap column was switched in line with the analytical column (Thermo Fisher Scientific, Amsterdam, Netherlands, PepMap C18, 500 mm × 75 μm ID, 3 μm, 100 Å). Peptides were eluted using a flow rate of 230 nl/min and a binary 1 h gradient, respectively 105 min.

The gradient starts with the mobile phases: 98% A (water/formic acid, 99.9/0.1, *v/v*) and 2% B (water/acetonitrile/formic acid, 19.92/80/0.08, *v/v/v*), increases to 35%B over the next 60 min, followed by a gradient in 5 min to 90%B, stays there for 5 min and decreases in 5 min back to the gradient 98%A and 2%B for equilibration at 30°C.

The Q Exactive Plus mass spectrometer was operated in data-dependent mode, using a full scan (*m/z* range 380–1,650, nominal resolution of 70,000, target value 3E6) followed by MS/MS scans of the 12 most abundant ions. MS/MS spectra were acquired using normalized collision energy of 27%, isolation width of 2.0 *m/z*, resolution of 17.500 and the target value was set to 1E5. Precursor ions selected for fragmentation (exclude charge state 1) were put on a dynamic exclusion list for 10 s. Additionally, the intensity threshold was calculated to be 4.0E4. The peptide match feature and the exclude isotopes feature were enabled.

Data processing protocol for analyzed peptides

For peptide identification, the RAW-files were loaded into Proteome Discoverer (version 1.4.1.14, Thermo Scientific). All hereby created MS/MS spectra were searched using MSAmanda v1.4.14.7870 (Dorfer *et al*, 2014). The RAW-files were searched against the SwissProt sequence database, using the taxonomy human (20,171 sequences; 11,317,551 residues). The following search parameters were used: beta-methylthiolation on cysteine was set as a fixed modification, oxidation on methionine, deamidation on asparagine and glutamine, acetylation on lysine, phosphorylation on serine, threonine and tyrosine and ubiquitination on lysine were set as variable modifications. Monoisotopic masses were searched within unrestricted protein masses for tryptic enzymatic specificity. The peptide mass tolerance was set to ± 5 ppm and the fragment mass tolerance to 0.03 Da. The maximal number of missed cleavages was set to 2. The result was filtered to 1% FDR on protein level using Percolator algorithm integrated in Thermo Proteome Discoverer. The localization of the post-translational modification sites within the peptides was performed with the tool ptmRS, based on the tool phosphoRS (Taus *et al*, 2011). Peptide areas have been quantified using in-house-developed tool apQuant (Doblmann *et al*, 2019).

In vitro ubiquitination assays

A method for in vitro ubiquitination assay is described elsewhere (Asaoka *et al*, 2016). Briefly, recombinant proteins of Ubiquitin (10 μg) (Sigma-Aldrich, U6253), mouse E1 (Ube1) (150 ng), human UbcH7 (300 ng), human HOIP (5 μg), human SHARPIN (1 μg), human-HOIL-1L (1 μg), human NEMO (5 μg), and ATP (2 mM) (Roche, 1051997900) were incubated in a reaction buffer consisting of 50 mM HEPES (Sigma-Aldrich, H4034) (pH7.5), 150 mM NaCl, 20 mM $MgCl_2$ for the indicated times at 37°C. Reactions were terminated by 2× SDS sample buffer at 96°C for 1 min. Samples were subjected to SDS–PAGE and subsequent immunoblotting.

In vitro deubiquitination assays (UbiCRest assays)

Deubiquitination assays were performed as previously described (Hospenthal *et al*, 2015). Briefly, recombinant deubiquitinases (3 μM for vOTU (CCHFV OTU domain, aa1–183), 10 μM for human OTULIN, 3 μM for human USP21 (USP domain, aa 196–565) were activated in activation buffer (150 mM NaCl, 25 mM Tris pH 7.5, and 10 mM DTT) for 10 min at room temperature. Subsequently,

samples in 10× DUB reaction buffer (500 mM NaCl, 500 mM Tris pH 7.5, and 50 mM DTT) were incubated with activated DUB for 30 min at 37°C. Reaction was terminated by 2× SDS sample buffer.

Bioinformatics analysis

A multiple sequence alignment of HOIP orthologues was performed with MAFFT (Katoh & Toh, 2008; Asaoka *et al*, 2016) and visualized using Jalview (Waterhouse *et al*, 2009).

qRT–PCR

A method is described elsewhere (Asaoka *et al*, 2016). 3×10^5 MEFs in 6-well plates were serum starved for 15 h in 0.2% FBS-DMEM, treated with human TNF (20 ng/ml) for the indicated timepoints. Samples washed by chilled PBS two times and the total RNA was extracted using TRIzol (Life Technologies, 15596018), treated with the TURBO DNA-free kit (Invitrogen, AM1907). 500 ng of RNA isolated from MEFs was reverse transcribed using oligo(dT)18 primer (New England Biolabs, #513165) and SuperScript II Reverse Transcriptase (Invitrogen, 18064-014). The cDNA was proceeded by using a standard qPCR method with GoTaq qPCR master mix (Promega, A6002) and the CFX96 Bio-Rad CFX 96 Real-Time PCR detection system. β-actin was used for normalization. Analysis was carried out using the $2^{-\Delta\Delta Ct}$ method. The sequences of primers used against mouse genes are as follows:

IκBα: forward primer 5′-GCTGAGGCACTTCTGAAAGCTG-3′, reverse primer 5′-TGGACTGGCAGACCTACCATTG-3′, ICAM: forward primer 5′-AAGGAGATCACATTCACGGTG-3′, reverse primer 5′-TTTGGGATGGTAGCTGGAAG-3′, VCAM: forward primer 5′-CTGGGAAGCTGGAACGAAGT-3′, reverse primer 5′-GCCAACACTTGACCGTGAC-3′, A20: forward primer 5′-AAAGGACTACAGCAGAGCCCAG-3′, reverse primer 5′-AGAGACATTTCCAGTCCGGTGG-3′, β-actin: forward primer 5′-CGGTTCCGATGCCCTGAGGCTCTT-3′, reverse primer 5′-CGTCACACTTCATGATGGAATTGA-3′.

Caspase activity assays

5×10^4 cells/well in a 96-well white plate (Thermo Scientific, 136101) were treated by human TNF (100 ng/ml), with or without cycloheximide (1 μg/ml) and z-VAD-fmk (20 μM). Caspase 3 or caspase 8 activity was measured according to the manufacturer's protocols by using the Caspase-3 Assay Kit (Fluorometric) (ab39383) or Caspase Glo 8 assay system (Promega, G8202), respectively. Signal was measured by a Synergy H1 microplate reader (Biotek Instruments, Inc) for the caspase 8 assays or using an EnSpire plate reader (Perkin Elmer) for the caspase 3 assays.

Live imaging analysis of caspase 3 activity

Detection of caspase3/7 activity was carried out using CellEvent™ Caspase-3/7 Green Detection Reagent (Thermo Scientific) following the manufacturer's protocol. Briefly, 4×10^4 cells per well were seeded per genotype and condition. SiR-Hoechst (100 nM) (a far-red DNA stain) was used as a marker for individual cells. Cells were stimulated with or without hTNF and the Caspase 3/7 Green Detection Reagent was added. Fluorescence was measured by using the cell discoverer 7 (Zeiss) over a period of 24 h.

ELISA assays

ProcartaPlex Immunoassays Kits (Thermo Fisher Scientific) were used to measure cytokine levels. Briefly, blood was collected from individual mice in BD Microtainer blood collection tubes (BD Microtainer SST tubes, Becton). Blood was centrifuged at $6,000 \times g$ for 8 min for plasma collection. Preparation of the standard curve generation and measurement of samples in duplicates were performed according to the manufacturer's protocol. The fluorescence intensity of each sample was read using the Luminex Analyzer (Merk).

Flow cytometry

Red blood cells in spleen homogenates and blood samples were lysed using ammonium-chloride-potassium (ACK) lysis buffer. Cells were then stained with a fixable Viability Dye eFluor780 (eBioscience, 65-0865-14) for 10 min at 4°C, were washed and blocked with CD16/CD32 Fc block (BD Bioscience, 553141) for 5 min at 4°C to inhibit unspecific antibody binding. Cells were labeled with antibodies in FACS buffer (PBS containing 2% fetal calf serum and 2 mM EDTA) on ice for 20 min. Intracellular staining was performed using the following antibodies CD19 (BD Biosciences, 563333), CD23 (eBioscience, 25-0232-82), CD93 (eBioscience, 62-5892-82), CD21 (BioLegend, 123411), TCRβ (BioLegend, 109205), NK1.1 (BD Biosciences, 557391) TCRβ (BD Biosciences, 553174), CD23 (Biolegend, 101620), DX5 (BD Biosciences, 558295), CD11b (BD Biosciences, 553312), B220 (BioLegend, 103221), CD28 (BioLegend, 122010), CD138 (BD Biosciences, 562935), CD45 (BioLegend, 103113), TCRβ (BD Biosciences,109229), CD4 (BioLegend, 100549), CD8 (BD Biosciences, 553035), CD44 (BD Biosciences, 550989), CD69 (BD Biosciences, 01504D), CD117 (BD Biosciences, 553355), CD11b (BioLegend, 101227), CD11c (BioLegend, 117335), Ly6G (BioLegend,127633), Ly6C (eBioscience,17-5931-81), F4/80 (BioLegend, 123131), TCRβ (BD Biosciences, 553170), and B220 (BD Biosciences, 553088). The samples were analyzed on an LSR II flow cytometer (BD). The data was analyzed using FlowJo software (Tree Star).

Generation and genotyping of C57BL/6J $Hoip^{K778R/K778R}$ knock-in mice

A method is described as previously (Wang *et al*, 2013). Briefly, the gRNA was designed using the online tool (crispr.mit.edu). Annealed oligonucleotide with gRNA targeting sequence was cloned into px330 plasmid by a standard subcloning method (Addgene plasmid, #42330, a gift from Feng Zhang (Cong *et al*, 2013)). The T7-gRNA product amplified by PCR was used as the template for *in vitro* transcription using the MEGAshortscript T7 kit (Invitrogen, AM1345). *In vitro* transcribed gRNA purified using the MEGAclear kit (Invitrogen, AM1908), Cas9 mRNA (Sigma CAS9MRNA-1EA), single strand oligonucleotide donor template containing K778R mutation, a silent mutation of the PAM sequence and a silent XmnI restriction site (ssOligo) (5′-TGCATCTTGTTCCCAGCTCAGAGAGAGCCTAGACCCCGATGCATATGCCCTGTTTCACAAGAGGCTGACCGAAGCTGTTCTTATGCGAGACCCCAAGTTCTTGTGGTGCGCCCAGGTAAACCTGACAAACAGAGTGAACT-3′) were used for injection. Superovulation-induced female C57BL/6J donor mice (3–5 weeks old), treated with

5 IU of pregnant mare's serum gonadotropin (PMSG) (Hölzel Diagnostika, OPPA01037) and subsequently with 5 IU of human chorionic gonadotropin (hCG) (Intervet, GesmbH), were mated and zygotes were isolated in M2 media (Merck Millipore, MR-015P-D) and cultured in KSOM medium (Cosmo Bio Co., Ltd, R-B074). The microinjection mix (100 ng/µl of Cas9 mRNA, 50 ng/µl of gRNA, 200 ng/µl of ssOligo) was microinjected into the cytosol of zygotes followed by transfer to pseudo-pregnant females. The genomic fragment of targeted region in $Hoip^{K778R/K778R}$ knock-in founder mice was confirmed by Sanger sequencing. Genotyping was performed by a PCR amplified genomic DNA fragment using forward primer 5′-CGATCCTCTTGCCTCCATGT-3′ and reverse primer 5′-CCAGCTGTTCGCGTTCATA-3′ was digested with XmnI (NEB; R0194L). Undigested and digested samples were proceeded for electrophoresis using 2% agarose gels.

Mouse husbandry

Mice were maintained in individually ventilated cages provided with HEPA filtered air (TECNIPLAST Green line GM 500) in a Light/Dark cycle (14 h light/10 h dark). Autoclaved food and water were provided ab libitum. Mice were housed under specific pathogen-free (SPF) conditions. The microbiological status of the mice was monitored by a sentinel program (soiled bedding sentinels and contact sentinels). $Hoip^{K778R/K778R}$ knock-in C57BL/6J mice, $Sharpin^{cpdm/cpdm}$ C57BL/KaLawRij (Ikeda et al, 2011), and $Tnfrsf1a^{tm1Mak}$/TNFRp55-deficient C57BL/6J mice (JAX stock #002818) were used in this study. For the breeding, the following program was used. $Hoip^{+/K778R}$ C57BL/6J female and male mice, or $Hoip^{K778R/K778R}$ C57BL/6J female and male mice were crossed with $Sharpin^{+/cpdm}$ male and female mice, which were backcrossed with C57BL/6J mice. $Hoip^{+/K778R}; Sharpin^{+/cpdm}$ male and female mice obtained from these crosses were then crossed to obtain all genotypes required for analysis and were bred to maintain the mouse line. This mouse line was maintained by breeding $Hoip^{+/K778R}; Sharpin^{+/cpdm}$ male and female mice together, which were obtained from different litters. $Hoip^{+/K778R}; Sharpin^{+/cpdm}$ female mice were crossed with $Tnfr1^{-/-}$ male mice. $Hoip^{+/K778R}; Sharpin^{+/cpdm}; Tnfr1^{+/-}$ male and female mice obtained from these crosses were then crossed to obtain all genotypes required for analysis and were bred to maintain the mouse line. This mouse line was maintained by breeding $Hoip^{+/K778R}; Sharpin^{+/cpdm}; Tnfr1^{+/-}$ male and female mice and $Hoip^{+/K778R}; Sharpin^{+/cpdm}; Tnfr1^{-/-}$ male and female mice together which were obtained from different litters. All animal procedures were conducted in accordance with European, Austrian, and institutional guidelines and protocols. All animal conduct was approved by local government authorities.

Histopathological analysis

A method is described elsewhere (Kumari et al, 2014). Briefly, dorsal and ventral skin, lung, spleen and liver and small intestine from mice were fixed in 10% neutral buffered formalin (Sigma, HT501128), processed with a microwave hybrid tissue processor (LOGOS, Milestone Medical), embedded in paraffin, sectioned (Microm, HM 355), and stained with hematoxylin and eosin in an automated stainer (Microm HMS 740). Immunohistochemistry was performed using an automated immunostainer (Bond III, Leica).

Primary antibodies used for immunohistochemistry were KRT14 (Sigma-Aldrich, SAB4501657, 1:200) CASP3, cleaved (Cell Signaling, 9661, 1:100) F4.80 (Bio-Rad, MCA497G, 1:100), Ly6G (Abcam, ab2557, 1:500) and secondary antibodies used are rabbit anti-rat IgG (Abcam, ab6733, 1:500), goat anti-rabbit IgG (Dako, E0432 1:500). The signal was detected with the Leica Bond Intense R Detection system. Slides were evaluated by a board-certified veterinary comparative pathologist with a Zeiss Axioskop 2 MOT microscope, and images were acquired with a SPOT Insight color camera (SPOT Imaging, Diagnostic Instruments, Inc.).

For the skin thickness measurement, digital images of sections stained with an KRT14 antibody were taken by the 3D Histech *Pannoramic Flash III* whole slide scanner and evaluated with the *Pannoramic Viewer* software. From each digital scene, 10 non-contiguous, representative foci were selected from a region spanning 4 mm. In each focus, the thickness of the entire epidermis, keratin layer, and squamous cell layer was measured. Measurements were tabulated, and the average of ten measurements was recorded per sample.

Mouse embryo analysis

Female mice mated with male mice of breeding age were checked for copulation plugs daily. The embryos were collected at different embryo stages (E12.5 and E13.5) and fixed in 10% neutral-buffered formalin (Sigma, HT501128) for 12–24 h at room temperature. Fixed embryos washed with PBS were imaged using a Lumar-Florescence Stereomicroscope with a color SPOT camera at 9× magnification.

Statistical analysis

Analysis was performed by the GraphPad Prism 8 software (GraphPad Software, Inc), and the mean values with standard deviation are shown. ANOVA test and Tukey's *post hoc* test were used. The significance and confidence level were set at 0.05, and P values are indicated in each figure legends as well as the number of replicates used to calculate statistics.

Data availability

The mass spectrometry proteomics data have been deposited to the ProteomeXchange Consortium via the PRIDE (Perez-Riverol et al, 2019) partner repository with the dataset identifier PXD021217 (http://www.ebi.ac.uk/pride/archive/projects/PXD021217).

Expanded View for this article is available online.

Author contributions

LMF performed the majority of the experiments, analyzed data, made figures and contributed to writing the manuscript, CGD contributed to the experiments, editing of figures and manuscript required for the revision, LD expressed and purified recombinant proteins required for *in vitro* assays, AK performed histological analysis, DH and AH performed FACS analysis, KY contributed to the IKK activity analysis, AS analyzed amino acid sequences of HOIP orthologues and made alignment, KM contributed to the mass spectrometry analysis, JMP supervised and contributed to the project planning, and FI performed caspase 3 assays and initial assays of the NF-kB reporter and mass spectrometry, supervised, planned and conducted the project, analyzed data, made figures, wrote the manuscript, and obtained funding.

Conflict of interest

The authors declare that they have no conflict of interest.

References

Akimov V, Barrio-Hernandez I, Hansen SVF, Hallenborg P, Pedersen AK, Bekker-Jensen DB, Puglia M, Christensen SDK, Vanselow JT, Nielsen MM *et al* (2018) UbiSite approach for comprehensive mapping of lysine and N-terminal ubiquitination sites. *Nat Struct Mol Biol* 25: 631–640

Akutsu M, Ye Y, Virdee S, Chin JW, Komander D (2011) Molecular basis for ubiquitin and ISG15 cross-reactivity in viral ovarian tumor domains. *Proc Natl Acad Sci USA* 108: 2228–2233

Ang RL, Ting AT (2018) Detection of RIPK1 in the FADD-containing death inducing signaling complex (DISC) during necroptosis. In *Programmed necrosis: methods and protocols*. Ting AT (ed.), pp 101–107. New York, NY: Springer

Asaoka T, Ikeda F (2015) New insights into the role of ubiquitin networks in the regulation of antiapoptosis pathways. *Int Rev Cell Mol Biol* 318: 121–158

Asaoka T, Almagro J, Ehrhardt C, Tsai I, Schleiffer A, Deszcz L, Junttila S, Ringrose L, Mechtler K, Kavirayani A *et al* (2016) Linear ubiquitination by LUBEL has a role in *Drosophila* heat stress response. *EMBO Rep* 17: 1624–1640

Boisson B, Laplantine E, Prando C, Giliani S, Israelsson E, Xu Z, Abhyankar A, Israel L, Trevejo-Nunez G, Bogunovic D *et al* (2012) Immunodeficiency, autoinflammation and amylopectinosis in humans with inherited HOIL-1 and LUBAC deficiency. *Nat Immunol* 13: 1178–1186

Boisson B, Laplantine E, Dobbs K, Cobat A, Tarantino N, Hazen M, Lidov HG, Hopkins G, Du L, Belkadi A *et al* (2015) Human HOIP and LUBAC deficiency underlies autoinflammation, immunodeficiency, amylopectinosis, and lymphangiectasia. *J Exp Med* 212: 939–951

Cong L, Ran FA, Cox D, Lin S, Barretto R, Habib N, Hsu PD, Wu X, Jiang W, Marraffini LA *et al* (2013) Multiplex genome engineering using CRISPR/Cas systems. *Science (New York, NY)* 339: 819–823

Damgaard RB, Walker JA, Marco-Casanova P, Morgan NV, Titheradge HL, Elliott PR, McHale D, Maher ER, McKenzie ANJ, Komander D (2016) The deubiquitinase OTULIN is an essential negative regulator of inflammation and autoimmunity. *Cell* 166: 1215–1230.e20

Doblmann J, Dusberger F, Imre R, Hudecz O, Stanek F, Mechtler K, Durnberger G (2019) apQuant: accurate label-free quantification by quality filtering. *J Proteome Res* 18: 535–541

Dorfer V, Pichler P, Stranzl T, Stadlmann J, Taus T, Winkler S, Mechtler K (2014) MS Amanda, a universal identification algorithm optimized for high accuracy tandem mass spectra. *J Proteome Res* 13: 3679–3684

Dove KK, Klevit RE (2017) RING-Between-RING E3 ligases: emerging themes amid the variations. *J Mol Biol* 429: 3363–3375

Draber P, Kupka S, Reichert M, Draberova H, Lafont E, de Miguel D, Spilgies L, Surinova S, Taraborrelli L, Hartwig T *et al* (2015) LUBAC-recruited CYLD and A20 regulate gene activation and cell death by exerting opposing effects on linear ubiquitin in signaling complexes. *Cell Rep* 13: 2258–2272

Elliott PR, Nielsen SV, Marco-Casanova P, Fiil BK, Keusekotten K, Mailand N, Freund SM, Gyrd-Hansen M, Komander D (2014) Molecular basis and regulation of OTULIN-LUBAC interaction. *Mol Cell* 54: 335–348

Elliott PR, Leske D, Hrdinka M, Bagola K, Fiil BK, McLaughlin SH, Wagstaff J, Volkmar N, Christianson JC, Kessler BM *et al* (2016) SPATA2 links CYLD to LUBAC, activates CYLD, and controls LUBAC signaling. *Mol Cell* 63: 990–1005

Emmerich CH, Ordureau A, Strickson S, Arthur JS, Pedrioli PG, Komander D, Cohen P (2013) Activation of the canonical IKK complex by K63/M1-linked hybrid ubiquitin chains. *Proc Natl Acad Sci USA* 110: 15247–15252

Fiil BK, Damgaard RB, Wagner SA, Keusekotten K, Fritsch M, Bekker-Jensen S, Mailand N, Choudhary C, Komander D, Gyrd-Hansen M (2013) OTULIN restricts Met1-linked ubiquitination to control innate immune signaling. *Mol Cell* 50: 818–830

Gerlach B, Cordier SM, Schmukle AC, Emmerich CH, Rieser E, Haas TL, Webb AI, Rickard JA, Anderton H, Wong WW *et al* (2011) Linear ubiquitination prevents inflammation and regulates immune signalling. *Nature* 471: 591–596

Haas TL, Emmerich CH, Gerlach B, Schmukle AC, Cordier SM, Rieser E, Feltham R, Vince J, Warnken U, Wenger T *et al* (2009) Recruitment of the linear ubiquitin chain assembly complex stabilizes the TNF-R1 signaling complex and is required for TNF-mediated gene induction. *Mol Cell* 36: 831–844

Heger K, Wickliffe KE, Ndoja A, Zhang J, Murthy A, Dugger DL, Maltzman A, de Sousa EMF, Hung J, Zeng Y *et al* (2018) OTULIN limits cell death and inflammation by deubiquitinating LUBAC. *Nature* 559: 120–124

Helmut B, Hildburg B, Gross HJ (1987) Improved silver staining of plant proteins, RNA and DNA in polyacrylamide gels. *Electrophoresis* 8: 93–99

Hospenthal MK, Mevissen TET, Komander D (2015) Deubiquitinase-based analysis of ubiquitin chain architecture using Ubiquitin Chain Restriction (UbiCRest). *Nat Protoc* 10: 349

Hrdinka M, Fiil BK, Zucca M, Leske D, Bagola K, Yabal M, Elliott PR, Damgaard RB, Komander D, Jost PJ *et al* (2016) CYLD Limits Lys63- and Met1-linked ubiquitin at receptor complexes to regulate innate immune signaling. *Cell Rep* 14: 2846–2858

Hrdinka M, Gyrd-Hansen M (2017) The Met1-linked ubiquitin machinery: emerging themes of (De)regulation. *Mol Cell* 68: 265–280

Ikeda F, Deribe YL, Skånland SS, Stieglitz B, Grabbe C, Franz-Wachtel M, van Wijk SJL, Goswami P, Nagy V, Terzic J *et al* (2011) SHARPIN forms a linear ubiquitin ligase complex regulating NF-κB activity and apoptosis. *Nature* 471: 637

Ikeda F (2015) Linear ubiquitination signals in adaptive immune responses. *Immunol Rev* 266: 222–236

Iwai K, Yamanaka K, Kamura T, Minato N, Conaway RC, Conaway JW, Klausner RD, Pause A (1999) Identification of the von Hippel-lindau tumor-suppressor protein as part of an active E3 ubiquitin ligase complex. *Proc Natl Acad Sci USA* 96: 12436–12441

Justus SJ, Ting AT (2015) Cloaked in ubiquitin, a killer hides in plain sight: the molecular regulation of RIPK1. *Immunol Rev* 266: 145–160

Katoh K, Toh H (2008) Recent developments in the MAFFT multiple sequence alignment program. *Brief Bioinform* 9: 286–298

Keusekotten K, Elliott PR, Glockner L, Fiil BK, Damgaard RB, Kulathu Y, Wauer T, Hospenthal MK, Gyrd-Hansen M, Krappmann D *et al* (2013) OTULIN antagonizes LUBAC signaling by specifically hydrolyzing Met1-linked polyubiquitin. *Cell* 153: 1312–1326

Kim W, Bennett EJ, Huttlin EL, Guo A, Li J, Possemato A, Sowa ME, Rad R, Rush J, Comb MJ *et al* (2011) Systematic and quantitative assessment of the ubiquitin-modified proteome. *Mol Cell* 44: 325–340

Kirisako T, Kamei K, Murata S, Kato M, Fukumoto H, Kanie M, Sano S, Tokunaga F, Tanaka K, Iwai K (2006) A ubiquitin ligase complex assembles linear polyubiquitin chains. *EMBO J* 25: 4877–4887

Kumari S, Redouane Y, Lopez-Mosqueda J, Shiraishi R, Romanowska M, Lutzmayer S, Kuiper J, Martinez C, Dikic I, Pasparakis M *et al* (2014) Sharpin prevents skin inflammation by inhibiting TNFR1-induced keratinocyte apoptosis. *Elife* 3: e03422

Kupka S, De Miguel D, Draber P, Martino L, Surinova S, Rittinger K, Walczak H (2016) SPATA2-mediated binding of CYLD to HOIP enables CYLD recruitment to signaling complexes. *Cell Rep* 16: 2271–2280

Lamkanfi M, Festjens N, Declercq W, Vanden Berghe T, Vandenabeele P (2007) Caspases in cell survival, proliferation and differentiation. *Cell Death Differ* 14: 44–55

Lechtenberg BC, Rajput A, Sanishvili R, Dobaczewska MK, Ware CF, Mace PD, Riedl SJ (2016) Structure of a HOIP/E2~ubiquitin complex reveals RBR E3 ligase mechanism and regulation. *Nature* 529: 546–550

Meier P, Morris O, Broemer M (2015) Ubiquitin-mediated regulation of cell death, inflammation, and defense of homeostasis. *Curr Top Dev Biol* 114: 209–239

Mertins P, Qiao JW, Patel J, Udeshi ND, Clauser KR, Mani DR, Burgess MW, Gillette MA, Jaffe JD, Carr SA (2013) Integrated proteomic analysis of post-translational modifications by serial enrichment. *Nat Methods* 10: 634–637

Peltzer N, Rieser E, Taraborrelli L, Draber P, Darding M, Pernaute B, Shimizu Y, Sarr A, Draberova H, Montinaro A *et al* (2014) HOIP deficiency causes embryonic lethality by aberrant TNFR1-mediated endothelial cell death. *Cell Rep* 9: 153–165

Peltzer N, Darding M, Walczak H (2016) Holding RIPK1 on the ubiquitin leash in TNFR1 signaling. *Trends Cell Biol* 26: 445–461

Peltzer N, Darding M, Montinaro A, Draber P, Draberova H, Kupka S, Rieser E, Fisher A, Hutchinson C, Taraborrelli L *et al* (2018) LUBAC is essential for embryogenesis by preventing cell death and enabling haematopoiesis. *Nature* 557: 112–117

Peltzer N, Walczak H (2019) Cell death and inflammation – a vital but dangerous liaison. *Trends Immunol* 40: 387–402

Perez-Riverol Y, Csordas A, Bai J, Bernal-Llinares M, Hewapathirana S, Kundu DJ, Inuganti A, Griss J, Mayer G, Eisenacher M *et al* (2019) The PRIDE database and related tools and resources in 2019: improving support for quantification data. *Nucleic Acids Res* 47: D442–D450

Rahighi S, Ikeda F, Kawasaki M, Akutsu M, Suzuki N, Kato R, Kensche T, Uejima T, Bloor S, Komander D *et al* (2009) Specific recognition of linear ubiquitin chains by NEMO is important for NF-kappaB activation. *Cell* 136: 1098–1109

Reiley WW, Zhang M, Jin W, Losiewicz M, Donohue KB, Norbury CC, Sun SC (2006) Regulation of T cell development by the deubiquitinating enzyme CYLD. *Nat Immunol* 7: 411–417

Rickard JA, Anderton H, Etemadi N, Nachbur U, Darding M, Peltzer N, Lalaoui N, Lawlor KE, Vanyai H, Hall C *et al* (2014) TNFR1-dependent cell death drives inflammation in Sharpin-deficient mice. *Elife* 3: e03464

Rittinger K, Ikeda F (2017) Linear ubiquitin chains: enzymes, mechanisms and biology. *Open Biol* 7: 170026

Rosner D, Schneider T, Schneider D, Scheffner M, Marx A (2015) Click chemistry for targeted protein ubiquitylation and ubiquitin chain formation. *Nat Protoc* 10: 1594–1611

Sasaki K, Iwai K (2015) Roles of linear ubiquitinylation, a crucial regulator of NF-kappaB and cell death, in the immune system. *Immunol Rev* 266: 175–189

Sasaki Y, Fujita H, Nakai M, Iwai K (2015) Immunoblot analysis of linear polyubiquitination of NEMO. *Methods Mol Biol* 1280: 297–309

Schaeffer V, Akutsu M, Olma MH, Gomes LC, Kawasaki M, Dikic I (2014) Binding of OTULIN to the PUB domain of HOIP controls NF-kappaB signaling. *Mol Cell* 54: 349–361

Schneider P, Bodmer JL, Holler N, Mattmann C, Scuderi P, Terskikh A, Peitsch MC, Tschopp J (1997) Characterization of Fas (Apo-1, CD95)-Fas ligand interaction. *J Biol Chem* 272: 18827–18833

Seymour RE, Hasham MG, Cox GA, Shultz LD, Hogenesch H, Roopenian DC, Sundberg JP (2007) Spontaneous mutations in the mouse Sharpin gene result in multiorgan inflammation, immune system dysregulation and dermatitis. *Genes Immun* 8: 416–421

Smit JJ, Monteferrario D, Noordermeer SM, van Dijk WJ, van der Reijden BA, Sixma TK (2012) The E3 ligase HOIP specifies linear ubiquitin chain assembly through its RING-IBR-RING domain and the unique LDD extension. *EMBO J* 31: 3833–3844

Smit JJ, van Dijk WJ, El Atmioui D, Merkx R, Ovaa H, Sixma TK (2013) Target specificity of the E3 ligase LUBAC for ubiquitin and NEMO relies on different minimal requirements. *J Biol Chem* 288: 31728–31737

Smit JJ, Sixma TK (2014) RBR E3-ligases at work. *EMBO Rep* 15: 142–154

Stieglitz B, Morris-Davies AC, Koliopoulos MG, Christodoulou E, Rittinger K (2012) LUBAC synthesizes linear ubiquitin chains via a thioester intermediate. *EMBO Rep* 13: 840–846

Takiuchi T, Nakagawa T, Tamiya H, Fujita H, Sasaki Y, Saeki Y, Takeda H, Sawasaki T, Buchberger A, Kimura T *et al* (2014) Suppression of LUBAC-mediated linear ubiquitination by a specific interaction between LUBAC and the deubiquitinases CYLD and OTULIN. *Genes Cells* 19: 254–272

Taus T, Köcher T, Pichler P, Paschke C, Schmidt A, Henrich C, Mechtler K (2011) Universal and confident phosphorylation site localization using phosphoRS. *J Proteome Res* 10: 5354–5362

Tokunaga F, Sakata S, Saeki Y, Satomi Y, Kirisako T, Kamei K, Nakagawa T, Kato M, Murata S, Yamaoka S *et al* (2009) Involvement of linear polyubiquitylation of NEMO in NF-kappaB activation. *Nat Cell Biol* 11: 123–132

Tokunaga F, Nakagawa T, Nakahara M, Saeki Y, Taniguchi M, Sakata S, Tanaka K, Nakano H, Iwai K (2011) SHARPIN is a component of the NF-kappaB-activating linear ubiquitin chain assembly complex. *Nature* 471: 633–636

Wagner SA, Satpathy S, Beli P, Choudhary C (2016) SPATA2 links CYLD to the TNF-alpha receptor signaling complex and modulates the receptor signaling outcomes. *EMBO J* 35: 1868−1884

Walczak H (2011) TNF and ubiquitin at the crossroads of gene activation, cell death, inflammation, and cancer. *Immunol Rev* 244: 9−28

Walden H, Rittinger K (2018) RBR ligase-mediated ubiquitin transfer: a tale with many twists and turns. *Nat Struct Mol Biol* 25: 440−445

Wang H, Yang H, Shivalila CS, Dawlaty MM, Cheng AW, Zhang F, Jaenisch R (2013) One-step generation of mice carrying mutations in multiple genes by CRISPR/Cas-mediated genome engineering. *Cell* 153: 910−918

Waterhouse AM, Procter JB, Martin DM, Clamp M, Barton GJ (2009) Jalview Version 2–a multiple sequence alignment editor and analysis workbench. *Bioinformatics (Oxford, England)* 25: 1189−1191

Witt A, Vucic D (2017) Diverse ubiquitin linkages regulate RIP kinases-mediated inflammatory and cell death signaling. *Cell Death Differ* 24: 1160−1171

Ye Y, Akutsu M, Reyes-Turcu F, Enchev RI, Wilkinson KD, Komander D (2011) Polyubiquitin binding and cross-reactivity in the USP domain deubiquitinase USP21. *EMBO Rep* 12: 350−357

Zhang J, Stirling B, Temmerman ST, Ma CA, Fuss IJ, Derry JM, Jain A (2006) Impaired regulation of NF-kappaB and increased susceptibility to colitis-associated tumorigenesis in CYLD-deficient mice. *J Clin Investig* 116: 3042−3049